U.S. DEPARTMENT OF THE INTERIOR

U.S. GEOLOGICAL SURVEY

GENERATION OF MAGMAS OF THE PIONEER BATHOLITH: A GEOLOGICALLY CONSTRAINED THERMAL MODEL

by

E-an Zen

U.S. Geological Survey 1/

Open-File Report 96-98

1/ Present address: Department of Geology, University of Maryland, College Park, Maryland 20742

TABLE OF CONTENTS

INTRODUCTION 4

ACKNOWLEDGMENTS 6

TECTONIC FRAMEWORK 6

- Tectonic Framework for the Pioneer Mountains 6
- Age and Timing of Tectonism 8
- Depth of Burial 9
- Decompression Rate 11

MODELLING; CONSTRAINTS FROM PETROLOGICAL DATA 13

- Inferred Nature of the Source Rock 13
  - Petrographic Information 13
  - Initial Strontium Isotope Ratios 14
  - Lead Isotope Data 15
  - Oxygen Isotope Data 17
  - Some Preliminary Inferences 17
- Observed Petrologic Relations 20

MODELLING: CONSTRAINTS FROM ENERGY CONSIDERATIONS 21

- Mode of Energy Transport into the Zone of Anatexis 21
- Crustal Heat Productivity 22
- Redistribution of U, Th and K During Crustal Anatexis 23

SELECTION OF MODEL PARAMETERS 26

- Variables, Mainly Tectonic 26
  - Decompression Rate 26
  - Thrust Advance Rate 26
- Variables, Mainly Thermal 27
  - Depth to the Interface of Thermal Perturbation 27
  - Incubation Period 28
  - Source Rock Heat Productivity 29
  - Estimating the Paleo-Subcrustal Heat Flux 31
  - Estimating the Peclet Number 33
  - Thermal Conductivity 33
  - Site-specific Thermal Parameters 34
- Variables, Mainly Concerning Melting Properties 34
- Summary of Modelling Procedure 35

MODEL RESULTS 37

FURTHER CONCLUSIONS FROM MODEL RESULTS 39

Subduction versus Mantle Upwelling 39

Significance of the Initial Strontium Ratio Values 40

REFERENCES CITED 42

TABLE CAPTIONS 48

TABLE 1 Models for cooling of plutons at WPRS 49

TABLE 2 Model ages of Source Terranes 50

TABLE 3 Parameters Used in Thermal Modelling and Results 51

TABLE 4 U and Th Contents of Southwest Montana Granitic Rocks and Some Comparisons 56

TABLE 5 K_2O, U, and Th Contents and Heat Productivity of Pioneer Batholith Rocks 57

FIGURE CAPTIONS 58

Figure 1 Index Map 60

Figure 2 Schematics of Tectonic Events 61

Figure 3 Nominal Cooling History as Function of Depth of Intrusion 62

Figure 4 SiO_2 vs. Th and U Contents 63

Figure 5 Th, U, vs. K_2O Contents 64

Figure 6 Wt % SiO_2 vs $K_2O/(K_2O+Na_2O)$ 65

Figure 7 SiO_2 and K_2O vs Heat Productivity 66

Figure 8 Possible distributions of heat productivity with depth 67

Figure 9 Temperarature Evolution for Model Runs 68

INTRODUCTION

The petrologically complex Pioneer batholith of southwestern Montana is located several hundred kilometers from the contemporaneous edge of the North American craton, and was emplaced during the waning stages of the Late Cretaceous Laramide orogeny. The Pioneer batholith is one of a group of batholiths -- the Philipsburg, the Tobacco Roots, the Sapphire, the Flint Creek, and the large Boulder batholiths -- in southwestern Montana that bear similar geological, age, and petrological stamps. In a setting of comparative crustal stability, identification of a feasible source of energy for the generation of voluminous magmas is a problem. Could heating that resulted from supracrustal thickening by thrusting (Zen, 1988a; Patiño-Douce and others, 1990) be the cause of anatexis, or would some other cause be required by the physical, chemical, and field-based geological and geochronological constraints? The present study attempts to explore the plausible thermal causes for the plutonic rocks by one-dimensional thermal modelling, using the general approach of Zen (1988a), but with model parameters constrained by field stratigraphic and tectonic relations as well as by actual chemical, age, and isotopic data that point to the nature of the source rocks for the magmas.

One-dimensional thermal models have severe limitations because lateral mass and energy transfer cannot be treated and because tectonic and intrusive events must be considered as instantaneous without possibility of premonitory or follow-up effects. Fortunately, the Pioneer batholith developed on the stable craton, and the known Cretaceous events can be reasonably assigned to en

bloc vertical motion and to the emplacement of thrust sheets, both of which, at least on a local scale, can be treated as one-dimensional problems.

I will first summarize the geological setting of the Pioneer batholith and next infer, from chemical and petrological data, the nature and thermal properties of the source terranes. I will then deduce values of variables to be used in modelling, such as uplift rates, the nature and number of thrust sheets, and relative timing of thrust emplacement and intrusion. I will present model results using reasonable input parameters and will suggest some constraints on the thermal history leading to the formation of the batholith. I will argue that shallow subduction cannot cause adequate melting in any reasonable time frame; upwelling of lithospheric mantle material is needed even to generate an amount of magma barely adequate to account for the batholith. Moreover, I will show that the physical properties of the system are such that the tectonic trigger of the anatectic event must have preceded the intrusion by several tens of millions of years. This requirement of a significant time lag between the triggering tectonism and magmatic events at shallow crustal levels applies to all regional geologic syntheses that include crustal derivation of magmas through conductive heating.

Modelling a real geological event by computer is akin to depicting a wild animal in a stylized frieze. The artist must first study minutely the anatomy and locomotion of the animal in its natural setting. Although such mastery does not ensure that he will capture the animation of a diving eagle or a racing cheetah, without careful field observation the frieze can never be better than a

caricature. The viewer will have to judge how well I have succeeded.

ACKNOLEDGMENTS

I thank Simon Peacock, Mike Ryan, and especially Ralph Haugerud for discussions of the pitfalls and promises awaiting thermal modellers. Discussions of igneous petrogenesis over the years with Joe Arth, Fred Barker, Paul Bateman, Zell Peterman, Frank Spera, Bob Tilling, Pete Toulmin, and Pete Wyllie have been instructive. Barney Berger, Larry Snee, and Jane Hammarstrom have been fellow travellers in my study of the Pioneer batholith, and I thank them for their discussions, help, and unfailing kindnesses. Thorough and constructive reviews by Bob Tilling and Ralph Haugerud have greatly improved this paper; Haugerud suggested backarc spreading as an alternative to subduction as the source of heating. I acknowledge their help with gratitude.

This manuscript was prepared in 1988-89; decision to place the report in the public domain through the medium of the Open-File Report came late. I have made no attempt to bring the data and interpretation current; however, I refer to reader to a published paper that is in many ways a summary of the information and ideas contained in this paper (Zen, 1992).

TECTONIC FRAMEWORK

Tectonic Framework for the Pioneer Mountains

The east and west branches of the Pioneer Mountains are separated by the aligned valleys of Wise River and Grasshopper Creek (Figure 1). A short distance east of the valley floor, the Fourth

of July high-angle normal fault downdropped the west side by several kilometers (and may have produced the graben valley of Wise River). This fault is the real tectonic boundary; however, for convenience I will use the physiographic terms to refer to the two tectonic blocks in the ensuing discussion. Though the two blocks have somewhat different histories, they are tectonically related; thermal modelling must consider their shared as well as distinct geology and chronology.

In the west Pioneer Mountains, two allochthonous sheets of Proterozoic sedimentary rocks have been thrust over the Phanerozoic rocks (the higher, Pattengail thrust sheet, PT, and the lower, Wise River thrust sheet, WRT, Figures 1 and 2). In the east Pioneer Mountains, only the Wise River thrust sheet is recognized (Zen, 1988b). Thus, rocks underlying the thrust sheets in the west Pioneers were tectonically buried deeper; because the thrust sheets were westerly derived, this tectonic burial also began earlier. The largest known pluton in the batholith, the Late Cretaceous Uphill Creek Granodiorite, spans both branches of the Pioneer Mountains (Snee, 1982). If, as is assumed, the pluton intruded the two parts simultaneously, then the time period of thermal relaxation between thrusting and plutonism, prior to regional uplift leading to the exhumation of the pluton in the Oligocene (Zen, 1988b), would be longer in the west Pioneers than in the east Pioneers. This timing difference has significant thermal consequences.

Two reference sites, called the West Pioneer Reference Site (WPRS) and the East Pioneer Reference Site (EPRS) (see below), were chosen to model the disparate thermal histories.

Age and Timing of Tectonism

In the east Pioneers, the Wise River thrust sheet predates the well-dated 72-Ma Uphill Creek Granodiorite and Grayling Lake Granite (Zen, 1988b; Myers, 1952; Sharp, 1970; Snee, 1978; for ages, see Marvin and others, 1983; Snee, 1982; Zen and others, 1975). Along the Wise River, the Stine Creek pluton, having a biotite ^{40}Ar-^{39}Ar spectrum age of 74.8 Ma and a biotite K-Ar age of 72.6 Ma (Zen, 1988b; Marvin and others, 1983), cuts the Wise River thrust west of the Fourth of July fault.

At least in the area of immediate interest, the emplacement of the Wise River sheet terminated the deposition of the uppermost Cretaceous sediments that was previously referred to as the Colorado Group (Zen, 1988b) but that will be denoted in this study as the undifferentiated Upper Cretaceous Fluviatile Sedimentary Rocks, UKFS. These sediments do not contain detritus that could be attributed to the allochthon; conglomerates that could be derived from the thrust sheets are stratigraphically higher (Zen, 1988b). Thus, the younger age limit of the pre-thrust sedimentary rocks is critical in dating the arrival of the thrust sheets.

In the uppermost recognized part of UKFS, palynomorphs were found in shale beds that indicated a middle Campanian to Maastrichtian age. Palmer (1983) gave the range of the Campanian Stage as 84.0-74.5$\pm$4 Ma, so that "middle Campanian" should be about 80 Ma. These ages are to be compared with the igneous ages of 72-75 Ma, given above. As both the radiometric ages and the palynomorphic determination may have an uncertainty of $\pm$5 m.y., the time gap

between the end of UKFS sedimentation and the intrusion cutting at least the Wise River thrust is no more than 10 m.y.. The thrusting event must fit within this gap, and its thermal role must be evaluated within this framework.

The Keokirk Quartz Diorite, a small pluton related to the main granodiorites of the batholith by identical initial strontium ratios (Arth and others, 1986), was emplaced at about 80 Ma, thus presumably during deposition of UKFS. The Keokirk, at the present level of exposure, cuts strata as young as late Paleozoic and stratigraphically about 3 km below the top of UKFS, so it is a very shallow intrusion. Clearly, the thrusting event was not the cause of the magma genesis, even though the thrust sheets, by thickening the crust by some 6-16 km, would have provided an extra, late-stage boost of heating for a region already undergoing fusion.

Depth of Burial

Snee (1982) first proposed that the west Pioneers were buried deeper than the east Pioneers from consideration of ^{40}Ar-^{39}Ar spectra data. Snee found that the Uphill Creek Granodiorite near Odell Mountain (the West Pioneer Reference Site, WPRS; Figure 1) gave a hornblende argon spectrum age older than the biotite argon spectrum age by 3.9 m.y.. In the Browne's Lake area (the East Pioneer Reference Site, EPRS; Figure 1), however, the same mineral pair from the same pluton gave a spectrum discordance of only 1.5 m.y. Intermediate discrepancies characterize the plutons between these sites. Snee (1982) interpreted the data in terms of the depth-dependence of the time needed to cool the rocks in each area through the range of closure temperatures for argon diffusion in

hornblende (about 540°C) and in biotite (about 280°C). Snee's depth estimates assumed a linear correlation between depth and the time it took to cool the rocks through the indicated temperature interval. Taking the emplacement depth at EPRS to be 3 km, Snee estimated that the pluton now exposed at WPRS was emplaced at a depth of 8 km. However, the method is sensitive to the reference depth chosen; if the emplacement depth at EPRS is taken to be 4 km, Snee's method would then predict WPRS to have been 11 km deep.

I tested Snee's estimate through a series of subsidiary thermal models. To make geologically useful comparisons of the apparent argon spectral ages ($\hat{=}t_{hb-bt}$), we must take into account the distance of the sample to its country-rock contact because, other factors being equal, a sample originally located well within the pluton would cool more slowly than one located near the contact. WPRS and EPRS are selected partly because both are situated about 0.5 km from their exposed country rock contacts. In my model calculations, I assumed a magma body 10 km thick, intruded instantaneously at 800°C into a static crust (i.e., no uplift) to produce a roof at a specified depth. I then examined the time required to cool from 540±20°C to 280±40°C. Figure 3 gives the calculated cooling curve ($\hat{=}t_{hb-bt}$ vs. depth to roof), along with Snee's linear model for two depths of EPRS, at 3 and at 4 km.

The model computation assumes that heat loss was by conduction; if convective cooling was significant, the model depth would be too shallow. Lack of evidence for wholesale hydrothermal alteration of the rocks in the west Pioneers suggest that convective cooling was not a major factor.

I also modelled the efficacy of a thick blanket of hot volcanic rock at WPRS to retard cooling of the pluton and result in a longer $\hat{}t_{hb-bt}$. The model blanketing layer of volcanic rocks was emplaced at the same time as the pluton; it was 3 km thick and initially at 550°C, except its base, which was taken to be initially at 275°C. The roof of the pluton was at 4 km, as at EPRS, so that a 1 km-thick layer of sedimentary rocks (at thermal equilibrium just prior to the magmatic events) intervened between the volcanic pile and the roof of the pluton. The results (Table 1) show that the increase in $\hat{}t_{hb-bt}$ is less than 1 m.y. even in the absence of uplift. A thick layer of hot volcanic rocks cannot explain the observed $\hat{}t_{hb-bt}$.

Snee (1988, oral commun.) estimated that the total pre-erosion thickness of thrust sheets in the west Pioneers was about 15 km (to be compared with model thickness of 16 km), implying that about 7 km of thrust sheets remain at the west Pioneer reference site. These values are schematically depicted to approximate vertical scale in Figure 2; the Fourth of July fault is assumed to have taken up all the relative vertical motion during both thrust loading and subsequent uplift. More precise definition of crustal uplift-erosion budget is not justified by the available data.

Decompression Rate

Field data bearing on rates of decompression (taken to equal erosion balanced by uplift) in the Pioneer Mountains are scanty, and the estimated rates are necessarily crude. EPRS is located near the bottom of the U-shaped Rock Creek valley, about 600 m below the general ridge crest, which is near the base of the Lower Cretaceous

Kootenai Formation (Zen, 1988b, cross sections J,L). Most of the relief of the gorge is the result of Quaternary valley glaciation; I assume that any pre-Eocene topographic relief did not significantly affect the thermobarometry of rocks then several kilometers below the surface. I further assume that, at the time of arrival of the Wise River thrust sheet, the full thickness of the Kootenai Formation was still preserved, as was at least part of the next higher unit, UKFS, that now underlies the allochthon at Morrison Hill. Thus, at least 1 km of these rocks plus a partial thickness of the overlying allochthon must be restored. This was the original basis for estimating a 4-km depth of intrusion. On the ridge east of Morrison Hill, an erosion surface coated by the 46-50 Ma (middle Eocene) volcanic rocks was developed on the allochthonous rocks at a level about 0.4-0.5 km above the thrust fault. These observations suggest about 2 km of erosion between the emplacement of the pluton at EPRS and Eocene volcanism about 20-25 m.y. later, yielding an average decompression rate of about 0.1 km/m.y. between 72 and 50 Ma. For lack of better data, I take this rate to apply to the period between the thrusting and plutonism as well.

Boulders of granite occur in a sequence of pumiceous ash and ash-matrix conglomerate on the north side of Fourth of July Ridge immediately west of the Fourth of July fault (Calbeck, 1975; Zen, 1988b, p. 20). The most probable source of the boulders is the 65-Ma (Late Cretaceous to Paleocene) Clifford Creek Granite that occurs just across the Fourth of July fault. Another outcrop of the ash farther south yielded a zircon fission-track age of 27 Ma (late Oligocene; Pearson and Zen, 1985). The Clifford Creek is another

high-level granite of the Pioneer batholith that cuts the thrust sheet. If a depth of intrusion of 4 km is assumed, an average uplift rate of 0.1 km/m.y. would just suffice to unroof the pluton by Oligocene time.

For WPRS, decompression rates are even harder to estimate. The overall average decompression rate must be about twice that for EPRS because the depth of intrusion of the now-exposed plutonic rocks was about twice as great. For this site, I used a model value of 0.2 km/m.y., though the actual rate during the early Tertiary could have been quite different.

MODELLING: CONSTRAINTS FROM PETROLOGICAL DATA

Inferred Nature of the Source Rock

Petrographic Information. Rocks of the Pioneer batholith commonly contain hornblende + biotite; they are metaluminous to barely peraluminous (the values of the aluminum saturation index, ASI, are mostly about 1; Zen, 1988c). The only rocks known to have ASI >1.1 are two late-stage leucocratic dikes (samples 315-1 and TKds) and a two-mica rock (sample BHS) interpreted to be a local differentiate of a nearly-metaluminous hornblende-bearing granodiorite (Zen, 1986). Rocks of the batholith typically contain abundant mafic inclusions and schlieren, but identifiable sedimentary xenoliths are rare. They have relatively high Na/K ratios; their oxide minerals are mainly magnetite (+ sphene) rather than ilmenite.

The petrography, especially the mafic mineralogy, as well as the lack of strongly peraluminous plutons suggest a source that was

either igneous or was already depleted of its most readily fusible components during the Cretaceous anatectic event. The emplacement of the batholith at high and relatively cold levels of the crust (3-4 km in the east Pioneers, possibly as high as 8 km in the west Pioneers) shows that the magmas must have been fairly dry until the end, when miarolitic cavities formed locally (Zen, 1988b), for otherwise the magmas would have frozen during ascent through decompression-induced loss of volatiles. These indications of a relatively nonfertile and dry source are consistent with the nature of the exposed Proterozoic and late Archaean rocks exposed in southwestern Montana: these are metasedimentary and metaigneous rocks now in the upper amphibolite to granulite facies of regional metamorphism (Sahinen, 1939; James and Hedge, 1980; Giletti, 1966; Lowell, 1965; Zen, 1988b). Presumably the source rocks were metamorphosed to at least as high grades as these exposed rocks.

Initial Strontium Isotope Ratios The inference that the source rocks for the Pioneer batholith must have been fairly dry and deficient in fertile material is complemented by the initial strontium ratios (iSr) of the batholith (Arth and others, 1986).

The iSr values of the Pioneer batholith range from a value of 0.7113 (Keokirk Quartz Diorite; Uphill Creek Granodiorite; Clifford Creek Granite) to 0.7160 (Trapper Tonalite). The highest value, $\geq$0.7304, was obtained from the two-mica aplite dike (sample 315-1) that also records the highest ASI value. These iSr values imply long crustal residence times for the source materials, and would seem to exclude appreciable mantle contribution of material to the magmas.

The iSr values of the Pioneer batholith stand in contrast to those of the Boulder batholith situated to the north-northeast. Rocks of the two batholiths are petrographically and chemically similar; they have the same age range and share comparable tectonic setting and history. The eastern limit of the batholiths together define a regional alignment; east of this alignment, as will be discussed, Laramide-age plutonism is negligible. However, the Boulder batholith (both the "Main Series" and the "Sodic Series" of Tilling, 1973) has much lower values of iSr (Doe and others, 1968), ranging from 0.7055 to 0.7092; an isopleth of 0.710 fully separates the two batholiths and this boundary is in fact mappable, at the present level of erosion, as the north-northwest-striking Sawmill Gulch-Trusty Gulch fault system (Figure 1; Zen, 1988b; for additional data on the satellite bodies of the Boulder batholith shown in Figure 1, see Arth and others, 1986; Zinter and others, 1983).

Lead Isotope Data Doe and others (1968) presented data on lead isotopes from the Boulder batholith. These data are augmented by new determinations (Doe and others, 1986) for both the Pioneer and Boulder batholiths. For the Pioneer batholith, the data are in part on whole rock, in part on feldspar (5 samples from various plutons), but predominantly on galena (and one cerrusite) from mineralized bodies associated with the Pioneer igneous event. The whole-rock sedimentary material were from different geographical areas and ages; the data form a scattered set. I treated the sets progressively as follows: (A) Igneous rock feldspar; (B) galena

from mineralized veins in igneous rocks; (C) galena and one cerussite from mineralized veins in country rocks (mainly sedimentary) adjacent to plutons; (D) sedimentary whole rocks. The sets are then progressively combined, (E) = (A) + (B); (F) = (E) + (C); and (G) = (D) + (F). The results (Table 2) show that the data sets are similar except for (D) which was therefore excluded from model age calculations. These calculations used the ISOPLOT program of Ludwig (1988).

The lead isotope data, exclusive of the sedimentary rocks, suggest a model source age of 1.9±0.2 Ga for the Pioneer batholith. This is younger than the age of the exposed Precambrian rocks in southwestern Montana (Giletti, 1966; James and Hedge, 1980) but is comparable with the age of a supracrustal unit of mixed biotitic plagioclase gneiss and hornblende-biotite amphibolite exposed in the area immediately north of the Pioneer batholith in the east Pioneer Mountains (Zen, 1988b, unit Xga). This unit has a metamorphic age (age of the last strontium homogenization) of about 1.6 Ga (Zen, 1988b; Arth and others, 1986), consistent with the 1.6-Ga regional metamorphism in southwestern Montana (Giletti, 1966); Pb-U ages on a zircon separated from the plagioclase gneiss gave apparent ages ranging from 1.1 to 1.8 Ga (Zen, 1988b), approaching the model age based on lead isotope data. The postulated antiquity of the source rock is compatible with the petrographic and iSr constraints, though it so far lacks independent support such as Nd/Sm dates.

The lead isotope data of the Boulder batholith (Doe and others, 1968, 1986) were used to calculate its model age. The result, 2.1±0.3 Ga, is not distinguishable from the model age for the

Pioneer batholith, and so on this basis the two batholiths could have had a common source terrane. I will later attempt to explain their different iSr values.

Oxygen Isotope Data These data are scanty for the Pioneer batholith. The values of ^{18}O range from 6.8 to 9.3 but are mostly less than 8 (J.R. O'Neil, 1979, written commun.); they are compatible with a lower crustal or upper mantle source, but not with a fertile sedimentary source.

Some Preliminary Inferences To summarize this discussion: it seems reasonable to assume that the major source of the magmas that constitute the Pioneer batholith was an old sialic crust. This source likely was ultimately at least in part sedimentary (to account for the high iSr), which either had already been depleted of its most fusible (peraluminous) components previous to the Late Cretaceous anatectic event, or had little or no peraluminous component. This source terrane is inferred to have been at the middle- to lower-crustal levels.

Three kinds of explanations for the different strontium isotope characteristics of the Boulder and the Pioneer batholiths can be suggested. The first is that the source terranes were unrelated and only fortuitously have the same lead isotope model age. The other explanations assume that the batholiths do share a common ultimate source, of Late Archaean or older age. The second explanation (see also Arth and others, 1986) is that the source terrane was isotopically homogenized during the 1.6 Ga regional thermal event that produced large-scale partial melting and segregation of the

terrane into melt-dominated "leucosomes" and restite-dominated "melanosomes". Each of these parts had enough volume to supply the material for a batholith. The leucosome-dominated terrane would have higher Rb/Sr ratios, a more rapid ^{87}Sr growth curve, and higher iSr values in Mesozoic time than would the melanosome-dominated terrane. These two parts became the sources respectively for the Pioneer and the Boulder batholiths, and the two sources supplied magma to discrete areas now separated now by the Trusty Gulch-Sawmill Gulch fault system.

The third possibility is that the Boulder batholith, with its lower iSr, incorporates more mantle-derived material during the Mesozoic anatectic event. The amount of material incorporated was not enough to affect the lead isotope data because the material is poor in common lead, but was enough to significantly lower the iSr. This model, depending on a postulated difference in leakage and mixing of material from the mantle, implies that energy transfer leading to the formation of the Boulder magmas was more efficient (see Huppert and Sparks, 1988) and could help explain the much larger size of that batholith.

Because the plutons of the Pioneer batholith are dominated by hornblende-biotite rocks, have an extended silica range typical of calkalkaline series, show no evidence of H_2O saturation except during the final stages of solidification, and must have been derived from an old source terrane already chemically depleted, the solidus temperature must have been at least 800^{o}C, and that melt generation must have been mostly in a vapour-absent regime, likely caused by the thermal breakdown of hydrous phases in the source

rocks.

The breakdown reactions leading to anatexis were discussed by many authors; in these discussions, the predicted temperature of appearance of melt widely varies, depending on the nature of the hydrous phase, the bulk composition of the system, and the database used to calculate the thermal stability of the hydrous phases in a melting situation. For example, Thompson and Tracy (1979) predicted partial melting of a pelitic system, using muscovite breakdown, in the temperature interval of 640-720°C, whereas Clemens and Vielzeuf (1987) predicted temperatures as high as 880-900°C for partial melting of quartzofeldspathic source rocks having biotite and hornblende as hydrous phases. They also predicted the production of large volumes of melt, exceeding 50 volume percent of the original bulk, mainly in response to biotite breakdown. In contrast, Patiño-Douce and others (1990) predicted much less melt generation for a similar source rock but having more hydrous phases. These volumetric estimates are important to our discussion not only because the plutons are sizable but because the critical melt fraction for melt separation (that is, the volume proportion of melt below which no accumulation and segregation as distinct magma bodies can happen) may be as large as 50% (see Miller and others, 1988; also Zen, 1988a, for review of experimental data and their interpretations).

Observed Petrologic Relations

Arth and others (1986) proposed at least three endmember magmas for the Pioneer batholith, having iSr values of 0.7112, 0.7138, and 0.7160. If these endmembers are real, they presumably were discrete

pods of magma formed in different parts of the source terrane. Mixing of the pods are observed at the level of intrusion, for example, the first two endmembers, represented by the Grayling Lake and the Uphill Creek plutons, locally mixed to form rocks of intermediate iSr along a broad contact zone between these two plutons (Zen, 1988b). Each magma also differentiated at depth, and the differentiates were sequentially intruded as more silicic and more peraluminous magmas; the volumetrically minor, mildly peraluminous granites (Clifford Creek Granite and some strongly peraluminous aplitic dikes) are late in the intrusive sequence. In the east Pioneers, all the plutons produced contact aureoles, commonly a few hundred meters wide. Taken together, these features mean that anatexis did not take place at the present level of erosion, and large magma reservoirs must have existed at some depth where processes of accumulation and differentiation had occurred.

Another kind of petrological constraint is furnished by the metamorphic grades of country rocks away from the plutonic contact. In the east Pioneers, away from the contact the rocks are little metamorphosed; shales and mudstones in UKFS contain smectite (Janet Hoffman, 1976, written commun.) and show no evidence of metamorphism, indicating a maximum temperature, at the present level of erosion, of no more than about 160°C (compare with model results, Table 3). In contrast, rocks near WPRS are reported to preserve pre-intrusion regional metamorphism in the lower amphibolite facies (L.W. Snee, 1988, oral commun.). However, because of the limited time available between thrust emplacement and plutonism (5-10 m.y., see p. 9), this metamorphism, if regional in extent, is unlikely to

be part of a burial-heating episode associated with the arrival of the thrust sheets. Although this metamorphism cannot provide effective constraints for thermal modelling, the model results (Table 3) for WPRS do predict regional temperatures at the present level of exposure as high as 300°C.

MODELLING: CONSTRAINTS FROM ENERGY CONSIDERATIONS

Mode of Energy Transport Into the Zone of Anatexis

Energy could be carried into the zone of anatexis and contribute to melting by several processes: Conduction (presumably from a subcrustal source; from "below" in 1-D modelling); advection, either as hot mafic magma or as a less viscous fluid phase from a hot and presumably higher-pressure region; and local production of heat through decay of radioactive elements, mainly K and the Th and U series.

For the Pioneer batholith, direct mixing of mantle magma as an agent of energy transport has already been ruled out on the basis of the isotope data. Even though the magmas must have been undersaturated in H_2O at the site of fusion, as discussed earlier, transport of energy by a fluid, possibly an aqueous fluid, from a hotter and presumably higher pressure region into the melt zone cannot be excluded *a priori*. If melting occurred in the lower crust, at pressures of about 8 kbar, then the experimental data (Wyllie, 1977a) would suggest no more than about 8-10 weight percent of H_2O in the final melt for hornblende and biotite to be stable but without a vapour phase. Much of this H_2O must be locally obtained through breakdown of hydrous phases (see Patiño-Douce and others,

1990; Vielzeuf and Hollowway, 1988). We will assume the fluid to be H_2O dominated because with its high heat capacity H_2O is an efficient energy carrier. *If* a source of pure H_2O could be found to contribute energy to the melt, it must also have dissolved in the understaturated melt in the process. As much as 3 weight percent of H_2O seems a reasonable upper bound for this source of H_2O. Assuming, generously, that this fluid came from a region at 1200°C and 10 kbar (improbable as this is geologically), about 10 weight percent of the source rock might be melted if the rock was already preheated to the solidus temperature (Burnham and others, 1969). Impressive as the figure may seem, the analysis is of the worst-case type, and even 10 percent melting, by itself, is not enough to cause melt mobilization. It would appear that the dominant mode of energy transport into the zone of anatexis must have been by conduction.

Energy locally generated by radioactive decay is not likely by itself to cause melting on a crustal scale, but could directly affect the quantity of melt because it modifies the thermal structure of the crust. What might be a reasonable value of crustal energy productivity, *A*, for the source terrane and for the crust as a whole?

Crustal Heat Production

The relation between observed surface heat flux and the heat productivity can be expressed by:

$$Q_f = Q_m + A.D$$

where Q_f is the observed surface heat flux, Q_m is the subcrustal contribution to the flux, *A* is the heat production rate in a slab of the crust, and D is a constant. Although in general *A* varies with

depth, a simple interpretation of the relations permitted by the data is that *A* is constant and D is the thickness of the heat-producing slab (Roy and others, 1968). This simple model is the mainstay of my calculations. The heat production rate, *A*, is assumed to extend over the upper 15 km of the original crust; it is also duplicated in the thrust sheets (Zen, 1988a).

The presence in the plutons of restitic minerals, such as zircon, that contains heat producing elements shows that the source region, most probably at depths greater than 15 km during the anatectic event, was not devoid of heat productivity, so the step-function relation, showing a sharp cutoff in the middle crust, cannot be strictly true, and some other distribution relation such as a logarithmic relation (Lachenbruch, 1970) may be better. However, changing the functional relation may affect the melt-producing property of the crust only indirectly. In a later section I will explore the effect on melt generation of different distributions of the heat productivity.

Redistribution of U, Th, and K During Crustal Anatexis

Of the three principal heat-producing elements in a sialic crust, potassium is hosted mainly by feldspar and mica (mainly biotite) at the metamorphic grade expected at an anatectic zone. These minerals can be expected to heavily dissolve into the melt; indeed the thermal breakdown of biotite, releasing H_2O, may be a major trigger for the initiation of the melting process (see Patiño-Douce and others, 1990; Vielzeuf and Holloway, 1988). The partitioning of uranium and thorium between the melt and the residual material (restite) is less obvious. Comparison of crustal

abundance data are risky because these data are for different kinds and ages of crustal rocks, including both potential source rocks and igneous rocks that could have been the result of anatexis. Even so, comparison of the Th and U contents of Archaean metamorphic rocks from the Beartooth Mountains, Montana that are less mafic than basalt (Wooden and others, 1988), of Archaean uraniferous granites of Wyoming (Stuckless and others, 1981), of "average crustal rocks": rocks of the Canadian shield, "average diorite and quartz diorite", and "average granodiorite" (all from Clark and others, 1966) with those of the Pioneer and Boulder batholiths (Table 4) shows similar values.

Thorium and uranium can be expected to be contained mainly in accessory phases of the source rocks, such as zircon, allanite, sphene, monazite, and apatite. These minerals must at least partly dissolve in an anatectic melt, but some, especially zircon and allanite, would also be entrained as restite phases. Thus, the efficacy of the entrainment process, which cannot be measured by phase-equilibrium studies, must be important in affecting the net partitioning of the heat producing elements. Empirically, we can examine the abundances of Th and U in granitic rocks and their source rocks, provided the petrogenetic connection between them can be demonstrated: not usually an easy undertaking. Migmatites are obvious candidates for such analysis if reliable Th and U data for leucosomes and melanosomes are available, although because of the small spatial separation of these bodies, segregation of dense restitic phases such as zircon and allanite through magma transport probably would not be noticeable.

Sawyer (1987) provided chemical data for the leucosome and melanosome of a migmatite complex in southwestern Ontario. The leucosome was considered to be the product of equilibrium partial melting of the source rock, and may include some entrained restite. The data indicate considerable enrichment of Th and U in the leucosome. In contrast, Weber and others (1985) showed that these elements were strongly retained in the melanosome in some migmatites of St. Malo, France, a finding in agreement with those of Barbey and others (1989) for the Telohat migmatite of Algeria. These data as a whole are equivocal.

The Cooma granodiorite complex of the Lachlan Fold Belt in southeastern Australia provides another view of these murky relations. The Cooma granodiorite is a small stock that has been considered to be produced by local anatexis of the Ordovician pelitic and psammitic sedimentary rocks that surround it, forming an extensive "regional metamorphic aureole" (Joplin, 1942, 1943; White and Chappell, 1977). Munksgaard's (1988) chemical data (Table 4) show virtually no distinction between the igneous and the sedimentary rocks in their Th and U abundances. These data suggest that in the anatectic event, Th and U, through dissolution into the melt and through entrainment in the product magma, was distributed evenly between the magma and the residual material.

Sawka and Chappell (1986) showed the K, U, and Th contents of 491 I-type and 316 S-type granitic rocks from the Lachlan Fold Belt of southeastern Australia as a function of the silica contents of the rocks. There is a slight covariance between Th, U and silica

for both rock types, and an expectable strong covariance between K and silica. These relations are consistent with the inference that during anatexis these heat-producing elements are at least not partitioned into the restite portion, so the heat productivity of a granite provides useful guides to those of the source rocks.

Combined with the tendency for potassium to enter the melt phase, I adopt as my working hypothesis that the heat productivity of the anatectic magma furnishes an upper estimate of that of the source rocks.

SELECTION OF MODEL PARAMETERS

The field and thermal constraints summarized above provide the basis to select values for variables used in modelling of anatexis of the Pioneer magmas using the "1DT" program of Haugerud (1986) and the technique described in Zen (1988a).

Variables, Mainly Tectonic

Decompression Rate As discussed before, the post-intrusion but pre-Eocene decompression rate at EPRS is estimated to be about 0.1 km/m.y. (0.1 mm/yr). For WPRS, a less-well constrained overall post-intrusion rate is 0.2 km/m.y. for the comparable time interval.

Thrust Advance Rate The model rate of advance of the thrust sheet is 7 km/m.y. (7 mm/yr) along the direction between the two reference sites. Using this value, it took 5 m.y. for the thrust sheet to traverse the 35 km between WPRS and EPRS. As a result, there is a 5-m.y.-longer wait between thrusting and magma intrusion at WPRS. A movement rate much less than 7 km/m.y. would be inconsistent with the ~10-m.y. "window" between cessation of Late

Cretaceous sedimentation and plutonism; a rate much greater for thrust movement seems unlikely. The time lapse between arrival of the two thrust sheets within the west Pioneers is unknown; an arbitrary value of 2 m.y. is used in the models. The thrust sheets are presumed to be surface- and over-stack thrusts; the older, lower sheet is 6 km thick and the younger, upper sheet is 10 km thick (Figure 2).

Variables, Mainly Thermal

Depth to the Interface of Thermal Perturbation In the model, thermal perturbation leading to anatexis is introduced instantaneously at a specified model depth, across which the new energy flux streams upward to modify the preexisting thermal profile. This "effective thermal interface" (ETI), therefore, is part of the lower boundary condition and is the depth at which the "mantle flux" is monitored in the computations. Physically, ETI could correspond to the depth of a subducted slab (Bird, 1988), or it could be the depth of something else such as the top of a hot spot representing upwelling of the asthenosphere. The thermal effect caused by an interface at a depth of 100 km and having a flux of 75 mWm^{-2} (e.g., depth of subduction modelled by Bird, 1988) would not be felt in the sialic crust (assumed to be 30 km thick initially) in less than about 70 m.y., requiring the subduction event to be no younger than 140-150 Ma, or Late Jurassic. Even an ETI of 75 km requires >50 m.y. for significant thermal response in the crust. It seems far-fetched to assume that a subducted oceanic slab and its lithosphere could maintain its thermal potency for such a long time, as a cooling slab would lose its efficacy rapidly.

Interface depths between 60 and 46 km (30 km of initial crust plus 16 km of thrust sheets) initiated about 40 m.y. prior to thrusting (i.e. ~110 Ma, corresponding to the beginning of accretion of terranes in western Idaho and eastern Oregon and Washington; see Lund and Snee, 1988) could produce sufficient volume of magma having the required melting temperature range.

Should there be a finite time lapse between the inception of ETI at the two reference sites? I modelled two possibilities: One, ETI began simultaneously at the two sites, and two, the time lag for ETI between the two sites was same as that for the arrival of the thrust sheets. For the latter alternative, the period of the first quiescent heating (incubation period ip_1; see below) would be the same at the two sites. Runs 10A, 10B, and 9G, Table 3, compare these results.

Incubation Period An incubation period (ip) in the model is any period when no tectonic event (including decompression) occurs, and the system undergoes static thermal relaxation to approach a new steady state. For the models used, the first incubation period, ip_1, is between the inception of ETI and the arrival of the first thrust sheet. The second one, ip_2, is between the arrival of the last thrust sheet and the beginning of decompression, assumed to be caused by erosion precisely balanced by uplift (Zen, 1988a; Haugerud and Zen, 1991). For WPRS a third incubation period ($ip_{1.5}$) intervenes between the arrival of the two thrust sheets.

In all the model runs, I arbitrarily set the inception of ETI at a model time of 3 m.y., assured in the following way. A steady-

state continental geotherm, terminating at model time of 3 m.y., was calculated and filed. In each subsequent model run, the filed data are used as the "prescribed geotherm" (Haugerud, 1986), so that thermal relaxation under the influence of enhanced mantle flux begins at 3 m.y. model time. Values of ip_1 used range between 15 and 40 m.y., i.e., thrusting begins between 18 and 43 m.y. into model time. As discussed already, values of ip_2 are 2 m.y. at EPRS and 5 m.y. at WPRS to assure synchroneity of uplift at the two sites. Value of $ip_{1.5}$ is fixed at 2 m.y.

Source Rock Heat Productivity The observed heat productivity of the plutons is assumed to be the upper limit for that of the source rock. No correction is made for the small difference between Late Cretaceous and modern radiogenic contents because the time interval is less than 10^8 years and the half lives of the relevant radioactive isotopes exceed 10^9 years.

Figures 4 and 5 give the available data on the K_2O, U, and Th contents of plutonic rocks of the Pioneer batholith. The U and Th abundances are plotted against SiO_2 and against K_2O in order to provide direct comparison with the data for the Boulder batholith (Tilling and Gottfried, 1969). For a given silica content, the maximum U and Th contents of the Pioneer batholith rocks generally are only about half of those of the Boulder batholith rocks (Figure 4); however, on a K_2O plot (Figure 5) this difference largely disappears, especially for Th abundance. This relation is consistent with the fact that the Pioneer plutons are generally less potassic than the "Main Series" of the Boulder batholith and are chemically similar to the "Sodic Series" (Figure 6; Tilling, 1973).

The low K_2O, Th, and U contents of the Pioneer rocks are consistent with deriving the metaluminous magmas from a radiogenic sialic source rock already depleted by previous anatexis.

These values are converted to heat productivity (Wetherill, 1966); I made no modification for improved isotopic abundances or decay constants since that publication. Figure 7 compares the heat productivity of the Pioneer batholith rocks with the average trend for the Boulder batholith of Tilling and others (1970). The unweighted average of the scanty data for the Pioneers is 2.11 ± 1.31 $uW.m^{-3}$ (N=18), or 1.85 ± 0.73 $uW.m^{-3}$ if an anomalously high value for sample BH9850 (a porphyritic border phase of the Grayling Lake pluton, Zen, 1988b) is excluded. The corresponding unweighted average content of silica is 69.4% and of K_2O is 3.4%; these two points are marked on Figure 7 by stars. For model use, I assigned a heat production value, *A*, of 1 $uW.m^{-3}$ for the source terrane, which is about half of the plutonic value. A 15-km thick radiogenic layer would contribute 15 $mW.m^{-2}$ to the pre-thrusting surface heat flux.

Finally, the effect of different distributions of the heat productivity in the crust needs to be explored (Figure 8). Most of the model runs (Figure 8) use a value of productivity, *A*=1 uWm^{-3} for the upper 15 km of the crust, and *A*=0 for greater depths. If *A*=0.5 for the entire 30 km of depth (compare Runs N11B and 524, Table 3), the volume of melt generated within 10 m.y. after uplift begins is as much as 20% greater. A third distribution, *A*=1 for Z=0, decreasing linearly to *A*=0 for Z=30 (thus keeping the total heat productivity constant; Run 526, Table 3), has intermediate effects on melt production. These differences are insignificant for our

discussion. Figure 8 also shows the exponential distribution of the same total heat productivity if A=1 at Z=0 (Lachenbruch, 1970). Although I cannot model this distribution, its effect would be comparable with the third alternative above. Table 3 also shows (Run 320) what would happen if A=1 for the entire 30 km of crust; the increase in melt production even for such a hot crust is only about 2/3 again as much.

Estimating the Paleo-Subcrustal Heat Flux Estimation of the subcrustal flux depends directly on the crustal productivity; it cannot be independently measured. Sclater and others critically reviewed existing data on heat flow on the continents and considered (1980, Table 7) the relation between the age of the craton and the observed heat flow. For North America as well as for the other continents, the average surface heat flow value for cratons >1.7 Ga is 46 $mW.m^{-2}$. Sclater and others (1980) also compiled the value of Q_m, the mantle flux, for different areas. For the continental interior the best value is one that Lachenbruch and Sass (1977) called the "eastern United States" value, 33 $mW.m^{-2}$, which accommodates observations in the stable central region of the United States. The difference between this and the cratonal heat flow of 46 $mW.m^{-2}$ is consistent with the heat production value of 1 $uW.m^{-3}$ for a 15-km thick productive crust chosen for the models. In round figures, I used a pre-subduction cratonal subcrustal flux of 30 $mW.m^{-2}$.

Another way to estimate the subcrustal heat flux in southwestern Montana is to consider modern-day values, obtained by plotting Q_f versus A for the rocks related by their common tectonic

provenance and extrapolating the data to A=0. No heat flow data exist for the Pioneer area, but a few data do exist for the Boulder batholith area (Blackwell and Robertson, 1973). Tilling (1974) reviewed the data, and showed that they cannot be interpreted unequivocally: even though the Boulder batholith data might be extrapolated to give a Q_m value of 75 $mW.m^{-2}$, they can equally well be interpreted as conforming to the regional Q_m value of 59 $mW.m^{-2}$ appropriate for the Basin and Range province (Lachenbruch and Sass, 1977). These authors pointed out the large scatter in the data for this province and showed that the entire province is characterized by anomalously high heat flow. This high regional heat flow for the Basin and Range province presumably reflects Tertiary and ongoing crustal extension; its Q_m value is not applicable to the Pioneer region prior to Late Cretaceous subduction.

For post-ETI mantle flux, I use values comparable with modern oceanic heat flow. The data of von Herzen and Lee (1969) suggest Q_m about 60 $mW.m^{-2}$ or slightly higher. Sclater and others (1980) showed the effect of age of the oceanic crust on the heat flow; a flux of 60 $mW.m^{-2}$ corresponds to a 45-Ma crust, but a flux of 75 $mW.m^{-2}$ requires a 15-Ma crust. My modelling results show that a flux of 60 $mW.m^{-2}$ would not produce adequate heating to generate large bodies of melts within the limited timespan required by the geological data; however, a flux of 75 $mW.m^{-2}$ does meet the needed rate of magma production.

Estimating the Peclet Number: Possible Coupling of Thermal and Tectonic Factors The motion of the thrust sheet might contribute frictional heat to the thermal regime. Oxburgh and Turcotte (1974)

and Peacock (1987) showed this effect to be negligible for all but the most local situations. However, coupling of conductive heating from below with convective heat transport by the movement of the thrust sheets could be important. This effect is evaluated by the Peclet number,

$$\underline{Pe} = U.l\ /k$$

where U is the speed of convective transport (here given by the rate of thrusting), *l* is a characteristic length (here given by the thickness of the thrust sheet), and k is the thermal diffusivity (Oxburgh and Turcotte, 1974). Using U of 7×10^{-3} m/year or 2.2×10^{-10} $m.s^{-1}$ (i.e., a thrust movement rate of 7 mm/year), *l* of 6×10^{3} m, and k of 8×10^{-7} $m^2.s^{-1}$, Pe becomes 1.6. Coupled energy transport probably cannot be ignored. Even so, however, if the fetch of both the ETI and thrusting are considerably greater than the distance between the two reference sites, as seems plausible, the thermal perturbation due to thrusting may be reasonably approximated for each site by a steady-state situation. If so, the coupled effects should be minor, and I have ignored them.

Thermal Conductivity A thermal conductivity, K, value of 2.00 $W.m^{-1}K^{-1}$ is used throughout. Although this value seems low, it is within the range of values tested by England and Thompson (1984), and does lead to slow thermal relaxation after the ETI event, whereas higher values of K result in lower crustal temperatures and less magma generation. A value for K=2.00 gives a thermal diffusivity value of $k=8 \times 10^{-7}$ $m^2.s^{-1}$. Density of 2780 $km.m^{-3}$ and heat capacity of 0.9 $kJ.kg^{-1}K^{-1}$ are used throughout.

Site-specific Thermal Parameters I assume that the crusts

underlying both parts of the Pioneer Mountains are substantially similar, so that the physical properties of the rocks such as original crustal thickness, thermal diffusivity, and heat productivity are the same for the two sites. However, the country rock temperatures at the two reference sites might have differed at the time of plutonism, as already described. For modelling purposes I constrain T ~160^{o} at the original (pre-thrust) land surface for EPRS and T >200^{o} at a level of land about 5 km above the original land surface for WPRS, both at the time of intrusion.

Variables, Mainly Concerning Melting Properties

The melting characteristics of the source terrane and of the anatectic magma must be estimated. I assume that the pressure of anatexis and of accumulation was greater than 5 kbar; i.e. at least 15 km below the land surface at that time). The temperature of the water-saturated solidus then becomes nearly independent of the total pressure. However, for reasons already discussed, the melt probably was not H_2O saturated, so fluid-absent reactions are envisioned to dominate the process of magma generation and the solidus must have been nearer 800^{o}C than 700^{o}C (see Wyllie, 1977a,b).

Considering the extended silica contents of the plutons, I allowed melting to occur in a temperature interval of 360^{o}C, at 10 fusion steps 40^{o}C apart, using a linear model such that as much as 10% of the rock may melt at each step (Zen, 1988a). Different solidus temperatures were tested (Table 3).

The heat of fusion used is the parametric value of Zen (1988a); $\hat{}h_f = \hat{}H_f/C_p$, where $\hat{}H_f$ is the heat of fusion and C_p is the heat

capacity. A value of $\hat{}h_f=3^oC$ per volumetric percent of melting is adopted. Heat of fusion prevents the crust from becoming as warm as it would be otherwise; however, *after* the crust has attained the steady-state temperature, in general only about one-third of the heat flux would be consumed in fusion; the bulk of the flux would be conducted away (if heat convection is important, then the fraction converted to latent heat can be expected to be even smaller; Zen, 1988a).

Summary of Modelling Procedure

The events and parameters for the models are sequenced as follows.

1. A steady state continental thermal profile is established for the original cratonic crust. The heat productivity, in most models confined to the upper 15 km, is 1 $uW.m^{-3}$; the mantle flux is 30 $mW.m^{-2}$. Thus the initial surface flux is 45 $mW.m^{-2}$.

2. The steady state is terminated by the instantaneous inception, 3 m.y. into model time, of a new and larger subcrustal thermal flux at a depth called the effective thermal interface, ETI, producing an upward flux of 75 $mW.m^{-2}$.

3. An incubation period, ip_1, follows; its duration ranges from 15 m.y. to 40 m.y., depending on the model, in order to produce temperatures high enough for anatexis.

4. ip_1 is terminated by the instantaneous arrival of the Wise River thrust sheet, 6 km thick, having physical and thermal properties of the upper 6 km of the original crust at that moment.

This thrust sheet arrived at West Pioneer Reference Site 5 m.y. earlier than at East Pioneer Reference Site. One set of models assumes that the inception of the ETI was instantaneous for the entire Pioneer region, whereas another set of models takes the time lag of inception of ETI at the two sites to be the same as that for the arrival of the thrust sheets, so that ip_1 was the same for the two reference sites.

5. A second, higher, Pattengail thrust sheet, 10 km thick, arrived at WPRS 2 m.y. later (after $ip_{1.5}$), possessing the thermal regime of the upper 10 km of the combined crust at that time and place.

6. A brief second period of quiescence, ip_2, followed at both sites. This period is longer at EPRS because the area did not receive the Pattengail sheet.

7. Uplift, exactly balanced by erosion, then proceeded in the entire Pioneer region. The rate is 0.2 km/m.y. for WPRS and 0.1 km/m.y. for EPRS.

The results of the model runs are examined for acceptability by using the field- and geochronometric constraints. At WPRS, the temperature at the present land surface (about 5 km above the pre-thrusting original land surface) may reach 300°C or even higher at the time of intrusion; however, at EPRS the temperature at the original land surface must never exceed about 160°.

MODEL RESULTS

Results of the modelling study are summarized in Table 3.

These data indicate the relative importance of the variables in controlling the volume of anatectic melt. Eight runs of Table 3 that produced melt are depicted in Figure 9, where the temperature record for four selected crustal depths are shown, located at 20, 25, and 30 km below the original surface, as well as right at the original surface (for EPRS) and at 5 km above the original surface (for WPRS); each record takes off from the equilibrium continental geotherm. Figure 9A relates the shape of the thermal curves to the benchmark tectonic events; from the time ticks on the curves isochrons can be readily constructed. Figures 9B through 9E show that if the mantle flux is changed from 75 to 60 $mW.m^{-2}$, with all other variables held the same, a 3-fold decrease in melt volume results at WPRS (Runs 9G, and 11B), and a nearly 5-fold decrease results at EPRS (Runs 10A and 11A). Figure 9F (Run 9A) illustrates the major effect of the depth of the thermal interface -- at ETI of 36 km, a large volume of melt resulted despite the high temperatures of the melting interval. Figures 9G (Run 10C) and 9H (Run 10B) and Figures 9C, 9I (Run 9F), and 9F are sets that show the effect of melting interval at the two sites. The kinks in the curves within melting intervals in part reflect the effect of stepwise and episodic melting (Zen, 1988a). For each run, I have marked the depth of the ETI and the regions where temperature becomes high enough to permit melting no more than 10 m.y. after the termination of ip_2 (to be consistent with the age constraints on tectonic events), using the assumed melting properties.

The volume of magma generated for EPRS, in even the most favourable models, is surprisingly small. Use of smaller latent

heat would increase the magma volume; $\hat{}h_f$ of 2^o would increase the magma volume by about 50%. One could argue reasonably that the volume of a typical plutonic rock contains much restite as well as earlier magmatic crystals whose precipitation "recycled" the thermal energy and caused continued melting. This is doubtless an important factor; its inclusion could augment the total magma by an uncertain but possibly substantial amount. Balanced against this factor, however, is the uncertain volume of melt that never pooled into the magma and intruded as part of the batholith. A nonlinear melting model could also change the volume of melt; the data of Vielzeuf and Holloway (1988) and of Patiño-Douce and others (1990) suggest lesser initial melt production than predicted by the linear model until biotite breaks down. The Pioneer batholith is at the eastern limit of the belt of Laramide-age magmatism; the paucity of model magma may reflect the reality of passing from a magma-producing to a magma-nonproducing environment. Moreover, the observed volume of magma at EPRS could in part reflect lateral magma transport. This line of argument highlights the weakness of one-dimensional models.

Because of the time constraints, thrusting could not have been the tectonic trigger for melting. However, during ip_1 prior to thrusting, the rate of heating decreases steadily; emplacement of the thrust sheets rejuvenates that rate and contributes to the generation of magma in the ensuing few tens of millions of years. The cessation of magma generation is accelerated by erosion; the scale of plutonism of a given region must depend on the rate of cooling and indirectly on the rate of decompression. Regionally, this factor could contribute to the differences among areas of

abundant, moderate, and little magmatism that are otherwise similarly situated relative to the late Mesozoic tectonic events.

FURTHER CONCLUSIONS FROM MODEL RESULTS

Subduction versus Mantle Upwelling

Bird (1988) provided an interesting two-dimensional model of tectonic evolution of the western United States between Late Cretaceous and Eocene time, consistent with known major plate-tectonic relations and the general tectonic features from the Rocky Mountains to the present Pacific coastal region. The model invokes a flat subducting plate, at a depth of about 100 km, that moved in a generally northeasterly direction; this plate eventually detached itself from the superjacent crust with the hinge line of detachment moving retrogressively southwestward during later parts of the Tertiary.

Bird's model predicts the location, time, and amount of crustal thickening due to this process; it also gives the arrival time, at any given spot, of the subducting oceanic lithosphere. For southwest Montana, Bird's model estimates its arrival between 75 and 60 Ma. These ages are too young to be relevant to the generation the magmas of the Pioneer batholith.

As my thermal models show, the depth of subduction must have been less than about 50 km in order to be effective. Because the Pioneer batholioth was located at least 300 km from the plate margin at that time (Armstrong and others, 1977; Lund and Snee, 1988), such a shallow depth would seem geologically and mechanically unrealistic; equally improbable is the maintenance, for as long as

30 m.y., of a subducted slab having the thermal characteristics of an oceanic crust no older than about 15 m.y. (i.e. flux of energy of about 75 mW/m^3; Sclater and others, 1980). I condlude that subduction was not a plausible cause of the increased subcrustal flux at the shallow ETI; rather, large-scale and sub-crustal mantle upwelling must be postulated.

Significance of the Initial Strontium Ratio Values

The initial strontium ratios for rocks of the Pioneer batholith do not permit much admixture of mantle material. For this batholith, the interaction between the anatectic zone in the lower crust and the subcrustal material must be confined to conductive energy transfer. For the Boulder batholith, in contrast, the consistently lower values of the initial strontium ratios do permit limited mixing of mantle material. Such leakage would enhance the efficiency of energy transfer from below (e.g., Huppert and Sparks, 1988). The average heat productivity of the Boulder batholith, nearly twice that of the Pioneer batholith, permits larger productivity value for its source. These two factors, taken together, could help to explain the much larger size of this batholith compared to the Pioneer batholith.

East of the alignment of the eastern margin of the two batholiths, Laramide-age plutonism decreases precipitously. The most notable exception of an appreciable size is the small Tobacco Roots batholith, similarly dominated by hornblende-biotite granodiorites. An initial strontium ratio for this body was reported (Shuster and others, 1989) to be 0.704, much lower than those of the two larger batholiths to the west, and well within the

range of values for the source regions of oceanic and magmatic-arc basalts expected for that age (Arth and others, 1986). Could the magmas of the Tobacco Roots batholith owe their existence to substantial leakage of mantle material and thus much enhanced efficiency of energy transfer?

Generation of magmas of the Pioneer and Boulder batholiths may have involved basically different geological processes than the vastly larger, tectonically outboard, and petrographically complex Idaho batholith, despite their comparable isotopic ages. The Idaho batholith consists largely of hydrous peraluminous (two-mica) granite (Hyndman, 1983) and has high iSr values (see review by Arth and others, 1986). I suggest that the Idaho batholith was truly subduction-related and "skimmed the cream" of the low-melting, hydrous, peraluminous fractions of the sediments. Such subducted sediments never reached the more inboard sites of the Pioneer and Boulder batholiths.

REFERENCES CITED

Armstrong, R.L., Taubeneck, W.H., and Hales, P.O., 1977, Rb-Sr and K-Ar geochronometry of Mesozoic granitic rocks and their Sr isotopic composition, Oregon, Washington, and Idaho: Geological Society of America Bulletin, v. 88, p. 397-411.

Arth, J.G., Zen, E-an, Sellers, George, and Hammarstrom, Jane, 1986, High initial Sr isotopic ratios and evidence for magma mixing in the Pioneer batholith of southwest Montana: Journal of Geology, v. 94, p. 419-430.

Barbey, Pierre, Bertrand, Jean-Michel, Angoua, Serge, and Dautel, Dannielle, 1989, Petrology and U/Pb geochronology of the Telohat migmatites, Aleksod, central Hoggar, Algeria: Contributions to Mineralogy and Petrology, v. 101, p. 207-219.

Bird, Peter, 1988, Formation of the Rocky Mountains, western United States: A continuum computer model: Science, v. 239, p. 1501-1507.

Blackwell, D.D., and Robertson, E.C., 1973. Thermal studies of the Boulder batholith and vicinity, Montana: Society of Economic Geologists, Butte [Montana] field meeting, August 1973, guidebook, p. D1-D8.

Burnham, C.W., Holloway, J.R., and Davis, N.F., 1969, Thermodynamic properties of water to 1000°C and 10,000 bars: Geological Society of America Special Paper 132, 96 p.

Calbeck, J.M., 1975, Geology of the central Wise River valley, Pioneer Mountains, Beaverhead County: Missoula, Montana, University of Montana, M.S. thesis, 89 p.

Clark, S.P., Jr., Peterman, Z.E., and Heier, K.S., 1966, Abundances of uranium, thorium, and potassium: p. 521-541 in S.P. Clark, Jr., editor, Handbook of physical constants, revised edition, Geological Society of America Memoir 97, 587 p.

Clemens, J.D., and Vielzeuf, D., 1987, Constraints on melting and magma production in the crust: Earth and Planetary Science Letters, v. 86, p. 287-306.

Doe, B.R., Berger, B.R., and Elliott, J.E., 1986, Lead-isotope evaluation of selected ores and mineral prospects in the Butte and Dillon 1° x 2° quadrangles, Montana: U.S. Geological Survey Open-File Report 86-111, 40 p.

Doe, B.R., Tilling, R.I., Hedge, C.E., and Klepper, M.R., 1968, Lead and strontium isotope studies of the Boulder batholith, southwestern Montana: Economic Geology, v. 63, p. 884-906.

England, P.C., and Thompson, A.B., 1984, Pressure-temperature-time paths of regional metamorphism, Pt. I, Heat transfer during the evolution of regions of thickened crust: Journal of Petrology, v. 25, p. 894-928.

Giletti, B.J., 1966, Isotopic ages from southwestern Montana: Journal of Geophysical Research, v. 71, p. 4029-4036.

Haugerud, R.A., 1986, 1DT - an interactive, screen-oriented microcomputer program for simulation of 1-dimensional geothermal histories: U.S. Geological Survey Open-File Report 86-511, 18 p.

Haugerud, R.A., and Zen, E-an, 1991, An essay on metamorphic path studies, or, Cassandra in P-T-t space: p. 323-348 in L.L. Perchuk, editor, Progress in metamorphic and magmatic petrology, University of Cambridge Press.

Huppert, H.E., and Sparks, R.S.J., 1988, The generation of granitic magmas by intrusion of basalt into continental crust: Journal of Petrology, v. 29, p. 599-624.

Hyndman, D.W., 1983, The Idaho batholith and associated plutons, Idaho and western Montana: Geological Society of America, Memoir 159, p. 213-240.

James, H.L., and Hedge, C.E., 1980, Age of the basement rocks of southwest Montana: Geological Society of America Bulletin, Pt. I, v. 91, p. 11-15.

Joplin, G.A., 1942, Petrological studies in the Ordovician of New South Wales, I. The Cooma Complex: The Linnean Society of New South Wales, Proceedings, v. 67, p. 156-196.

Joplin, G.A., 1943, Petrological studies in the Ordovician of New South Wales, II. The northern extension of the Cooma Complex: The Linnean Society of New South Wales, Proceedings, v. 68, p. 159-183.

Lachenbruch, A.H. 1970, Crustal temperature and heat production: implications of the linear heat-flow relations: Journal of Geophysical Research, v. 75, p. 3291-3300.

Lachenbruch, A.H., and Sass, J.H., 1977, Heat flow in the United States and the thermal regime of the crust: p. 626-675 in J.G. Heacock, editor, The earth's crust, its nature and physical properties: American Geophysical Union, Geophysical Monograph 20, 754 p.

Lowell, W.R., 1965, Geologic map of the Bannack-Grayling area, Beaverhead County, Montana: U.S. Geological Survey, Miscellaneous Geologic Investigations Map I-433, scale 1:31,680.

Ludwig, K.R., 1988, Isoplot for MS-DOS, a plotting and regression program for radiogenic-isotope data, for IBM-PC compatible computers, version 1.07: U.S. Geological Survey, Open-File Report 88-557, revised edition of May 2, 1989, 37 p.

Lund, Karen, and Snee, L.W., 1988, Tectonic development of the Salmon River suture zone, western Idaho: Conclusions and questions: Geological Society of America Abstracts with Programs, v. 20, p.

429.

Marvin, R.F., Zen, E-an, Hammarstrom, J.M., and Mehnert, H.H., 1983, Cretaceous and Paleocene potassium-argon ages of the northern Pioneer batholith and nearby igneous rocks in southwest Montana: Isochron/West, no. 38, p. 11-17.

Miller, C.F., Watson, E.B., and Harrison, T.M., 1988, Perspectives on the source, segregation, and transport of granitoid magmas: Royal Society of Edinburgh, Transactions, Earth Sciences, v. 79, p. 135-156.

Munksgaard, N.C., 1988, Source of the Cooma Granodiorite, New South Wales -- a possible role of fluid-rock interactions: Australian Journal of Earth Sciences, v. 35, p. 363-377.

Myers, W.B., 1952, Geology and mineral deposits of the northwest quarter, Willis quadrangle and adjacent Brown's Lake area, Beaverhead County, Montana: U.S. Geological Survey Open-File Report 147, 46 p., 2 plates.

Oxburgh, E.R., and Turcotte, D.L., 1974, Thermal gradients and regional metamorphism in overhtrust terrains with special reference to the eastern Alps: Schweizerische Mineralogische und Petrographische Mitteilungen, v. 54, p. 641-662.

Palmer, A.R., 1983, The Decade of North American Geology 1983 geologic time scale: Geology, v. 11, p. 503-504.

Patiño-Douce, A.E., Humphreys, E.D., and Johnston, A.D., 1990, Anatexis and metamorphism in tectonically thickened continental crust exemplified by the Sevier hinterland, western North America: Earth and Planetary Sciences Letters, v. 97, p. 290-315.

Peacock, S.M., 1987, Creation and preservation of subduction-related inverted metamorphic gradients: Journal of Geophysical Research, v. 92B, p. 12,763-12,781.

Pearson, R.C., and Zen, E-an, 1985, Geologic map of the east Pioneer Mountains, Beaverhead County, Montana: U.S. Geological Survey Miscellaneous Field Studies Map MF-1806-A, scale 1:50,000, with text.

Roy, R.F., Blackwell, D.D., and Birch, Francis, 1968, Heat generation of plutonic rocks and continental heat flow provinces: Earth and Planetary Science Letters, v. 5, p. 1-12.

Ruppel, E.T., O'Neill, J.M., and Lopez, D.A., 1983, Preliminary geologic map of the Dillon 1^{o} by 2^{o} quadrangle, Montana: U.S. Geological Survey Open-File Report 83-168, 1 sheet, scale 1:250,000.

Sahinen, U.M., 1939, Geology and ore deposits of the Rochester and adjacent mining districts, Madison County, Montana: Montana Bureau of Mines and Geology Memoir 19, 53 p.

Sawka, W.N., and Chappell, B.W., 1986, The distribution of radioactive heat production in I- and S-type granites and residual source regions: implications to high heat flow areas in the Lachlan Fold Belt, Australia: Australian Journal of Earth Sciences, v. 33, p. 107-118.

Sawyer, E.W., 1987, The role of partial melting and fractional crystallization in determining discordant migmatite leucosome compositions: Journal of Petrology, v. 28, p. 445-473.

Sclater, J.G., Jaupart, C., and Galson, D., 1980, The heat flow through oceanic and continental crust and the heat loss of the earth: Reviews of Geophysics and Space Physics, v. 18, p. 269-311.

Sharp, G.S., 1970, Stratigraphy and structure of the Greenstone Mountain area, Beaverhead County, Montana: Corvallis, Oregon, Oregon State University, M.S. thesis, 121 p.

Shuster, R.D., Mueller, P.A., D'Arcy, K., and Heatherington, A., 1989, Nd evidence of the age and nature of source regions of the northeastern Idaho batholith and Tobacco Root batholith, Montana: Geological Society of America, Abstracts with Programs, v. 21, p. 325.

Snee, L.W., 1978, Petrography, K/Ar ages, and field relations of the igneous rocks of part of the Pioneer batholith, southwestern Montana: M.A. thesis, Ohio State University, 110 p.

Snee, L.W., 1982, Emplacement and cooling of the Pioneer batholith, southwestern Montana: Ph.D. thesis, Ohio State University, 320 p.

Thompson, A.B., and Tracy, R.J., 1979, Model systems for anatexis of pelitic rocks, II, Facies series melting and reactions in the system $CaO-KAlO_2-NaAlO_2-Al_2O_3-SiO_2-H_2O$: Contributions to Mineralogy and Petrology, v. 70, p. 429-438.

Tilling, R.I., 1973, Boulder batholith, Montana - a product of two contemporaneous but chemically distinct magma series: Geological Society of America Bulletin, v. 84, p. 3879-3900.

Tilling, R.I., 1974, Estimating the "thickness" of the Boulder batholith, Montana, from heat-flow and heat-productivity data: Geology, v. 2, p. 457-460.

Tilling, R.I., and Gottfried, David, 1969, Distribution of thorium, uranium, and potassium in igneous rocks of the Boulder batholith region, Montana, and its bearing on radiogeneic heat production and heat flow: U.S. Geological Survey Professional Paper 614-E, 29 p.

Tilling, R.I., Gottfried, David, and Dodge, F.C.W., 1970, Radiogenic heat production of contrasting magma series: bearing on interpretation of heat flow: Geological Society of America Bulletin, v. 81, p. 1447-1462.

Vielzeuf, Daniel, and Holloway, J.R., 1988, Experimental

determination of the fluid-absent melting relations in the pelitic system: Contributions to Mineralogy and Petrology, v. 98, p. 257-276.

von Herzen, R.P., and Lee, W.H.K., 1969, Heat flow in oceanic regions: p. 88-95 in P.J. Hart, editor, The earth's crust and upper mantle: American Geophysical Union, Geophysical Monograph 13, 735 p.

Weber, C., Barbey, P., Cuney, M., and Martin, H., 1985, Trace element behaviour during migmatization. Evidence for a complex melt-residuum-fluid interaction in the St. Malo migmatitic dome (France): Contributions to Mineralogy and Petrology, v. 90, p. 52-62.

Wetherill, G.W., 1966, Radioactive decay constants and energies: p. 514-519 in S.P. Clark, Jr., editor, Handbook of physical constants, revised edition, Geological Society of America Memoir 97, 587 p.

White, A.J.R., and Chappell, B.W, 1977, Ultrametamorphism and granitoid genesis: Tectonophysics, v. 43, p. 7-22.

Wooden, J.L., Mueller, P.A., Mogk, D.A., and Bowes, D.R., 1988, A review of the geochemistry and geochronology of Archean rocks of the Beartooth Mountains, Montana and Wyoming: In S.E. Lewis and R.B. Berg, editors, Precambrian and Mesozoic plate margins: Montana, Idaho and Wyoming: Montana Bureau of Mines and Geology, Special Publication 96, p. 23-42.

Wyllie, P.J., 1977a, Crustal anatexis: an experimental review: Tectonophysics, v. 43, p. 41-71.

Wyllie, P.J., 1977b, From crucibles through subduction to batholiths: p. 389-433 in S.K. Saxena and Somdev Bhattacharji, editors, Energetics of geological processes, New York, Springer-Verlag, 473 p.

Zen, E-an, 1986, Aluminum enrichment in silicate melts by fractional crystallization: some mineralogic and petrographic constraints: Journal of Petrology, v. 27, p. 1095-1117.

Zen, E-an, 1988a, Thermal modelling of stepwise anatexis in a thrust-thickened sialic crust: Royal Society of Edinburgh, Transactions, Earth Sciences, v. 79, p. 223-235.

Zen, E-an, 1988b, Bedrock geology of the Vipond Park 15-minute, Stine Mountain 7-1/2 minute, and Maurice Mountain 7-1/2 minute quadrangles, Pioneer Mountains, Beaverhead County, Montana: U.S. Geological Survey Bulletin 1625, 49 p., 2 plates.

Zen, E-an, 1988c, Phase relations of peraluminous granitic rocks and their petrogenetic implications: Annual Reviews of Earth and Planetary Sciences, v. 16, p. 21-51.

Zen, E-an, 1992, Using granite to image the thermal state of the

source terrane: Royal Society of Edinburgh, Transactions, Earth Sciences, v. 83, p. 107-114.

Zen, E-an, Marvin, R.F., and Mehnert, H.H., 1975, Preliminary petrographic, chemical, and age data on some intrusive and associated contact metamorphic rocks, Pioneer Mountains, southwestern Montana: Geological Society of America Bulletin, v. 86, p. 367-370.

Zinter, G.G., Snee, L.W., and Sutter, J.F., 1983, Geology, petrology, and age of emplacement of the Big Hole Canyon intrusion near Dewey, southwest Montana: Geological Society of America, Abstracts with Programs, v. 15, p. 412.

TABLE CAPTIONS

Table 1. Comparison of results of a layer of hot volcanic rocks versus deep burial on the expected cooling rate of a pluton, as expressed by the difference in the hornblende and biotite argon cooling ages ($\hat{}t_{hb-bt}$), at the WPRS.

Table 2. Calculations of model ages of source terranes for the Pioneer and Boulder batholiths, based on lead isotope data. See text for details.

Table 3. Parameters used in thermal modelling calculations, and principal results. See text for discussion.

Table 4. Crustal abundances of uranium and thorium for various types of material, compared to those of the Pioneer and Boulder batholiths. Sources of data: Boulder batholith, Canadian shield rocks, and average crust, Tilling and Gottfried, 1969. Pioneer batholith, Zen, this study. Archaean granites of Wyoming, Stuckless and others, 1981. Archaean rocks of the Beartooth Mountains, Wooden and others, 1988. Other rocks, Clark and others, 1966. Quetico migmatite, Sawyer, 1987. Cooma granodiorite and metamorphic rocks, Munksgaard, 1988.

Table 5. K_2O, Th, and U contents of rocks of the Pioneer batholith, and heat productivity of the Pioneer batholith rocks, calculated by using the conversion factors of Wetherill (1966).

TABLE 1 MODELS FOR COOLING OF PLUTON AT THE WEST PIONEER REFERENCE SITE

Model-cell dimension (in the vertical direction): 1 km

Argon closure temperatures: Hornblende, 540°C
Biotite, 280°C

Monitoring depth for cooling record: 4.5 km (0.5 km below upper contact of intrusion)

Model 1. Effect of a hot ash layer overlying shallow intrusion

Thermal configuration: 0-2.5 km, 550°C
3.0 km, 275°C
3.5 km, equilibrium geotherm (75°C)
4.0-13.5 km, 800°C
>14 km, equilibrium geotherm

Mantle flux $mW.m^{-2}$	Apparent age difference, $\hat{=}t_{Hb-Bt}$, m.y. with ash	without ash, same depth of burial
30	1.6	1.6
75	2.7	2.4

Model 2. Effect of deep burial of intrusion by thrust sheet

Mantle flux: 30 $mW.m^{-2}$

Intrusion, roof level, km	Monitor depth, km	$\hat{=}t_{Hb-Bt}$, m.y.
10	10.5	7
9	9.5	5

TABLE 2. Model ages of source terranes for the Pioneer and the Boulder batholiths based on lead isotope data.

Type of material	Number of samples	Model 1	Model 2
Pioneer batholith			
A. Igneous rock	5	1520 +/- 1100	--
B. Vein in igneous rock	6	1680 +/- 710	1760 +/- 680
C. Vein in sedim. rock	16	1560 +/- 550	1820 +/- 470
D. Sedimentary wholerock	4	482 +/- 930	506 +/- 920
E. A+B	11	1670 +/- 430	1770 +/- 400
F. E+C	27	1720 +/- 260	1850 +/- 240
G. F+D	31	818 +/- 340	1010 +/- 300
Boulder batholith			
(1) Doe and others (1986), vein galena	26	1890 +/- 310	2060 +/- 280
(2) Doe and others (1968), size-controlled sample	9	1990 +/- 780	--

Table 3 Parameters used in thermal modelling, and principal results

Run No.	Incubation Period, m.y.a/ ip_1	$ip_{1.5}$	ip_2	Monitor Depth, kmb/	Melting Interval, °C	Maximum Ambient Temp., °Cc/	Total Fusiond/ End of ip_2	5 m.y. later	10 m.y. later
					EPRS				
N5A	35	--	2	36	700-1060	181	4.61	5.88	7.26
N1A	35	--	2	36	740-1100	182	3.73	4.88	6.21
N6A	35	--	2	36	800-1160	183	2.59	3.56	4.71
N3A	35	--	2	46	700-1060	164	2.17	3.15	4.31
N2A	35	--	2	46	740-1100	165	1.61	2.43	3.44
N4A	35	--	2	46	800-1160	166	0.81	1.42	2.24
625Ae/	35	--	2	46	800-1160	161	1.25	2.00	2.99
625Bf/	35	--	2	46	800-1160	162	0.96	1.60	2.44
N4AAg/	35	--	2	46	800-1160	166	0.81	1.40	2.23
N4BBh/	35	--	2	46	800-1160	166	0.81	1.42	2.20
527Ai/	35	--	2	46	800-1160	149	0.03	0.18	0.46
10Bj/	35	--	2	60	700-1060	143	0.31	0.71	1.34
10A	40	--	2	60	700-1060	144	0.58	1.10	1.80
11Ak/	40	--	2	60	700-1060	133	0.01	0.14	0.39
10C	35	--	2	60	740-1100	143	0.09	0.35	0.82
N7A	35	--	2	60	800-1160	143	0.00	0.05	0.29

Table 3 (continued)

Run No.	Incubation Period, m.y. a/ ip_1	$ip_{1.5}$	ip_2	Monitor Depth, km b/	Melting Interval, °C	Maximum Ambient Temp., °C c/	Total Fusion d/ End of ip_2	5 m.y. later	10 m.y. later
					WPRS				
N9B	35	2	5	46	700-1060	260	4.11	6.57	9.07
N10B	35	2	5	46	740-1100	262	3.23	5.43	7.90
9A	15	2	5	46	800-1160	248	0.61	2.03	3.96
9B	15	2	5	100	800-1160	170	0	0	0
N11B	35	2	5	46	800-1160	266	2.17	4.04	6.28
320l/	35	2	5	46	800-1160	297	4.65	7.55	10.22
524m/	35	2	5	46	800-1160	247	2.88	4.89	7.26
526n/	35	2	5	46	800-1160	249	2.36	4.11	6.18
9H	35	2	5	55	700-1060	239	1.74	3.34	5.37
527B	35	2	5	56	800-1160	241	0.41	1.33	2.70
527Co/	35	2	5	56	800-1160	217	0	0.13	0.55
9Gp/	35	2	5	60	700-1060	228	0.91	2.10	3.73
11Bq/	35	2	5	60	700-1060	228	0.10	0.54	1.29
9F	35	2	5	60	740-1100	228	0.54	1.42	2.83
N8B	35	2	5	60	800-1160	231	0.17	0.71	1.70
N12B	35	2	5	75	700-1060	202	0.00	0.24	0.80
9E	35	2	5	75	740-1100	201	0	0.05	0.42
N13B	35	2	5	75	800-1160	203	0	0	0.06
9C	35	2	5	100	740-1100	169	0	0	0
9Dr/	35	2	5	100	740-1100	163	0	0	0

Table 3 (continued)

Notes

a/ ip_1 as indicated. $ip_{1.5}$ is 2 m.y. (WPRS only). ip_2 is 2 m.y. at EPRS and 5 m.y. at WPRS.

b/ i.e., initial depth of thermal interface chosen to monitor mantle flux.

c/ For EPRS, at original land surface; for WPRS, 5 km above original land surface.

d/ Figures in these three columns represent equivalent thickness of residuum-free melt generated in the crustal column, in kilometers. See Zen (1988a). "Later" refers to time lapse since end of ip_2.

e/ Same as N4A, except that the heat production, A, is 0.5 $uW.m^3$ throughout the 30 km thickness, so that the integrated crustal production is same as for run N4A.

f/ Same as N4A, except that the heat production, A, is 1.0 $uW.m^3$ at Z=0 and decreases linearly to 0 at Z=30; the integrated crustal production is same as for run N4A.

g/ Thermal interface rises with uplift and at the same rate.

h/ Thermal interface rises with uplift and at the same rate; thermal flux across the interface decreases by 2.5 mWm^{-2} at 5 m.y. interval after uplift begins.

i/ Monitor depth decreases with uplift at 0.1 km/m.y. and $Q_m(2)$, starting at 60 mWm^{-2}, decreases by 2.5 mWm^{-2} for each 5 m.y. of uplift.

j/ Value of ip_1 is yoked to that of run 9G by assumed rate of advance of thrust sheet.

k/ $Q_m(2)$ is 60 $mW.m^{-2}$. Compare with run 10A.

l/ Same as run N11B except that the heat production, A, is 1 $uW.m^{-3}$ throughout the 30-km thickness, rather than just the upper 15-km thickness, of the crust.

m/ Same as run 320 except that the heat production, A, is 0.5 $uW.m^3$ throughout the 30 km thickness, so that the integrated crustal production is same as for run N11B.

n/ Same as run N11B except that the heat production, A, is 1.0 $uW.m^3$ at Z=0 and decreases linearly to 0 at Z=30; the integrated crustal production is same as for run N11B.

o/ Same as run 527B except that $Q_m(2)$ is 60 $mW.m^{-2}$ rather than 75 $mW.m^{-2}$.

p/ Value of ip_1 is yoked to those of runs 10A and 10B by assumed rate of advance of thrust sheet. See text for discussion.

q/ $Q_m(2)$ is 60 $mW.m^{-2}$. Compare with run 9G.

r/ Value of thermal conductivity used is 2.5 $W.m^{-1}K^{-1}$.

Table 3 (continued)

Other parameters used in modelling:

Dimensions of model cell: 1 km normally; 0.5 km where necessary.

Thermal conductivity: 2 $W.m^{-1}K^{-1}$

Heat production, A (upper 15 km only): 1 $uW.m^{-3}$.

Heat capacity, 0.9 $kJ.kg^{-1}.K^{-1}$.

Bulk density: 2780 $kg.m^{-3}$.

Thermal diffusivity, 8 x 10^{-7} $m^2.s^{-1}$.

Mantle flux before to subduction, $Q_m(1)$: 30 $mW.m^{-2}$.

Mantle flux after subduction, $Q_m(2)$: 75 $mW.m^{-2}$. See notes above.

Fusion Step: 40°C.

Parametric heat of fusion, $\hat{h}_f$ (Zen, 1988a): 300K

Time interval for adjusting thermal profile: 5 m.y.

First thrust sheet is 6 km thick; second thrust sheet is 10 km thick and is present only at WPRS.

Decompression (uplift balanced by erosion) rate for EPRS is 0.1 km/m.y.; for WPRS is 0.2 m.y.

Table 4 U AND Th CONTENTS OF SW MONTANA GRANITIC ROCKS AND SOME COMPARISONS (ppm)

	MEAN U		MEAN Th	
BOULDER BATHOLITH (n=60)	3.9		15.4	
PIONEER BATHOLITH (n=18)	3.2		14.0	
QUETICO MIGMATITE, CANADA				
Source metasediments (n=1)	2.6		6.7	
Equilibrium partial melt (n=3)	3.3		15.3	
COOMA AREA, AUSTRALIA				
Cooma granodiorite	3.5	(n=4)	18.8	(n=5)
High grade psammite	3.9	(n=7)	18.7	(n=7)
Low grade psammite	4.6	(n=5)	17.3	(n=7)
High grade pelite	5.0	(n=2)	20.7	(n=3)
Low grade pelite	4.3	(n=6)	18.7	(n=6)
ARCHAEAN METAMORPHIC ROCKS, BEARTOOTH MOUNTAINS (n=35)	1.7		9.1	
Details:				
Meta-andesite (n=9)	2.2		7.3	
Meta-pelite (n=2)	2.0		8.0	
Meta-dacite (n=18)	2.5		10.0	
Meta-rhyolite (n=3)	0.7		8.0	
Meta-greywacke (n=3)	1.7		24.3	
ARCHAEAN MAFIC GRANITE, WIND RIVER RANGE (n=46)	3.5		30.5	
AVERAGE DIORITE & QUARTZ DIORITE	2.0	(n=69)	8.5	(n=47)
AVERAGE GRANODIORITE	2.6	(n=156)	9.3	(n=92)
CANADIAN SHIELD ROCKS (n=330)	2.5		10.3	
AVERAGE CONTINENTAL CRUST	2.8		10.0	

TABLE 5 K_2O, U, Th contents and heat productivity of Pioneer batholith rocks (Heat production calculation based on Wetherill, 1966)

Sample	Rock Unit[a]	SiO_2 wt %	K_2O wt %	U ppm	Th ppm	Heat Production cal/g rock/yr			Total heat production	
						K_2O	U	Th	cal/g rock/yr	W/m^3[b]
315-1	Tda	74.3	4.6	6.3	27.4	1.03	4.60	5.48	11.11	3.98
516-1	Tqp	70.9	3.1	1.1	8.1	0.69	0.80	1.62	3.12	1.12
500-1	TKc	72.34	3.97	2.6	10.4	0.89	1.90	2.08	4.87	1.74
32-1-1	TKc	75.4	4.6	1.9	5.2	1.03	1.39	1.04	3.46	1.24
BC	Kbc	69.5	2.7	1.4	5.7	0.60	1.02	1.14	2.77	0.99
BHS	Kgl	72.8	3.5	1.8	13.9	0.78	1.31	2.78	4.88	1.75
1228-1	Kgl	68.5	3.2	2.5	11.4	0.72	1.83	2.28	4.82	1.73
1293-1	Kgl	68.4	3.2	2.4	8.5	0.72	1.75	1.70	4.17	1.49
1293-2	Kgl	69.8	3.1	2.7	10.9	0.69	1.97	2.18	4.85	1.73
1298-2	Kgm	67.9	3.3	3.8	16.7	0.74	2.77	3.34	6.85	2.45
BH9850	Kgp	64.7	2.8	9.2	54.4	0.63	6.72	10.88	18.22	6.52
744-2	Kgb	71.9	3.6	3.1	15.4	0.81	2.26	3.08	6.15	2.20
121-1	Kuc	65.5	3.5	6.8	11.2	0.78	4.96	2.24	7.99	2.86
IVP	Kuc	65.04	3.03	2.6	10.8	0.68	1.90	2.16	4.74	1.70
1272-2	Kuc	68.9	3.2	3.6	9.9	0.72	2.63	1.98	5.32	1.91
881-1	Kuc	66.4	3.4	2.2	10.1	0.76	1.61	2.02	4.39	1.57
1162-1	Ksc	70.7	3.6	1.9	13.3	0.81	1.39	2.66	4.85	1.74
547-1	Kt	61.27	2.26	1.6	8.6	0.51	1.17	1.72	3.39	1.22
Average [c]		69.4	3.4	3.2 (2.8)	14.0 (11.6)					2.11 (1.85)

[a] Using designations of Zen (1988b)
[b] Using bulk density value of 2700 $kg.m^{-3}$
[c] For use in Figure 7. Data between parentheses exclude sample BH9850.

FIGURE CAPTIONS

Figure 1. Index map showing distribution of plutons and other geological features referred to in the text. The East Pioneer Reference Site (EPRS) and the West Pioneer Reference Site (WPRS) are indicated. Geological features in the area between 45°30' and 45°45'N and between 112°45' and 113°7'30"W are generalized from Zen (1988b); areas outside are generalized from Ruppel and others (1983), and from Snee (1982). Area underlain by plutons are ornamented. Areas underlain by rocks of the Wise River thrust sheet (WRT) are shown separately only east of the Fourth of July fault system.

Figure 2. Schematic representation of the sequence of thrusting, erosion, igneous intrusion, and high-angle faulting in the Pioneer Mountains. (A), arrival of the thrust sheets. (B), emplacement of the plutons; their tops are arbitrarily set at the present level of erosion. (C), displacement on the Fourth of July fault system downdropping the west Pioneer block. (D), erosion to the present time. EPRS and WPRS are the two reference sites. Dotted lines schematically connect the panels for the west and east Pioneers. Long dashed lines on (B) are the original surfaces of the thrust sheets, and the distance between a given dashed line and the next lower solid line defines the amount of crust removed by erosion up to the specified time. The upper thrust plate rests on the Pattengail thrust (PT); the lower thrust plate rests on the Wise River thrust (WRT; Zen, 1988b), which rests on the autochthon (AC).

Figure 3. Nominal cooling history of a pluton given by the difference between the argon spectrum ages of hornblende and biotite ($\hat{}t_{hb-bt}$), as a function of depth of intrusion. Distance from sample location (WPRS) to the margin of the pluton, assumed to be the roof, is 0.5 km. Solid curve, calculated from conduction model of heat flow. Dashed curves, linear cooling model used by Snee (1982).

Figure 4. SiO_2 versus thorium and uranium contents of the Pioneer batholith rocks, and comparison with the Boulder batholith rocks shown generalized as a distribution field (Tilling and Gottfried, 1969).

Figure 5. Thorium and uranium contents versus K_2O content of Pioneer batholith, and comparison with the Boulder batholith rocks shown generalized as a distribution field (Tilling and Gottfried, 1969). The number "3" refers to triplication of data points.

Figure 6. Weight percent SiO_2 versus $K_2O/(K_2O+Na_2O)$ plot of Pioneer batholith rocks (circles) and of the Proterozoic gneiss-and-amphibolite unit (Xga, crosses), compared to the Main Series (solid line) and the Sodic Series (dashed line) of the Boulder batholith (Tilling, 1973). The number "2" refers to duplication of data points.

Figure 7. (A) SiO_2 and (B) K_2O contents versus heat productivity. Comparison of Pioneer batholith rocks with those of the Boulder batholith, shown as the trend line given by Tilling and others (1970). Average values for the Pioneer batholith rocks (n=17) excluding one anomalous value are given by stars.

Figure 8. Four possible distributions of heat productivity, A, in the crust. (A), A=1 $uW.m^{-3}$, confined to the upper 15 km only, A=0 below that depth. (B), A=0.5 $uW.m^{-3}$, distributed throughout the 30 km of crust, so that the integrated value of A for the entire crust remains the same. (C), A=1 $uW.m^{-3}$ at Z=0, decreasing linearly to A=0 at Z=30, so that the integrated value of A for the entire crust remains the same. (D), $A=A_o e^{-Z/D}$; where A_o=1 $uW.m^{-3}$ and D=18.825, so that the integrated value of A for the entire crust remains the same.

Figure 9. Temperature evolution at chosen depths for selected runs. (A), key that relates tectonic events and incubation periods to changes in the curves. (B), Run 10A. (C), Run 9G. (D), Run 11A. (E), Run 11B. (F), Run 9A. (G), Run 10C. (H), Run 10B. (I), Run 9F. See text for discussion; see Table 3 for model parameters.

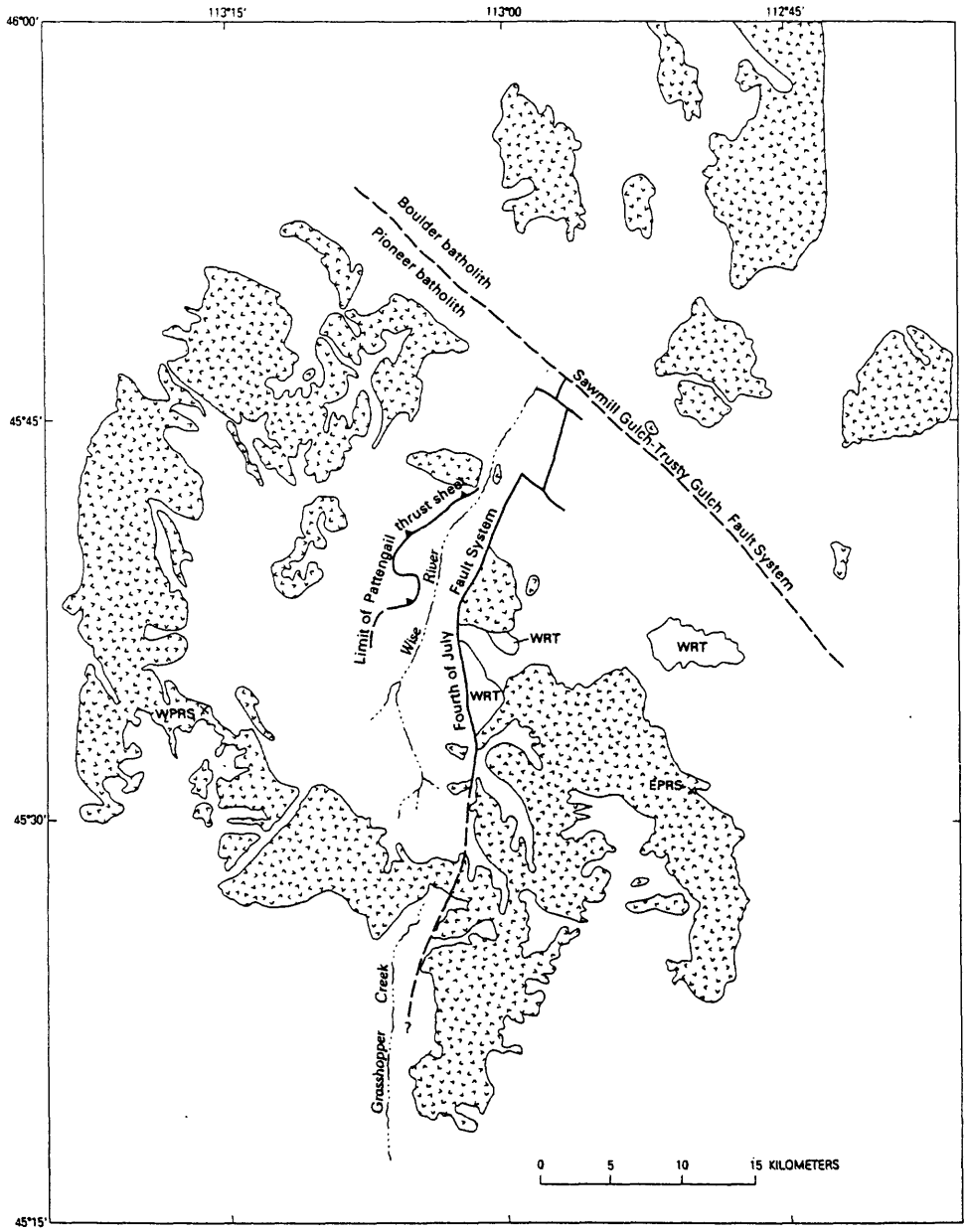

Figure 1. Index map showing distribution of plutons and other geological features referred to in the text. The East Pioneer Reference Site (EPRS) and the West Pioneer Reference Site (WPRS) are indicated. Geological features in the area between 45°30' and 45°45'N and between 112°45' and 113°7'30"W are generalized from Zen (1988b); areas outside are generalized from Ruppel and others (1983), and from Snee (1982). Area underlain by plutons are ornamented. Areas underlain by rocks of the Wise River thrust sheet (WRT) are shown separately only east of the Fourth of July fault system.

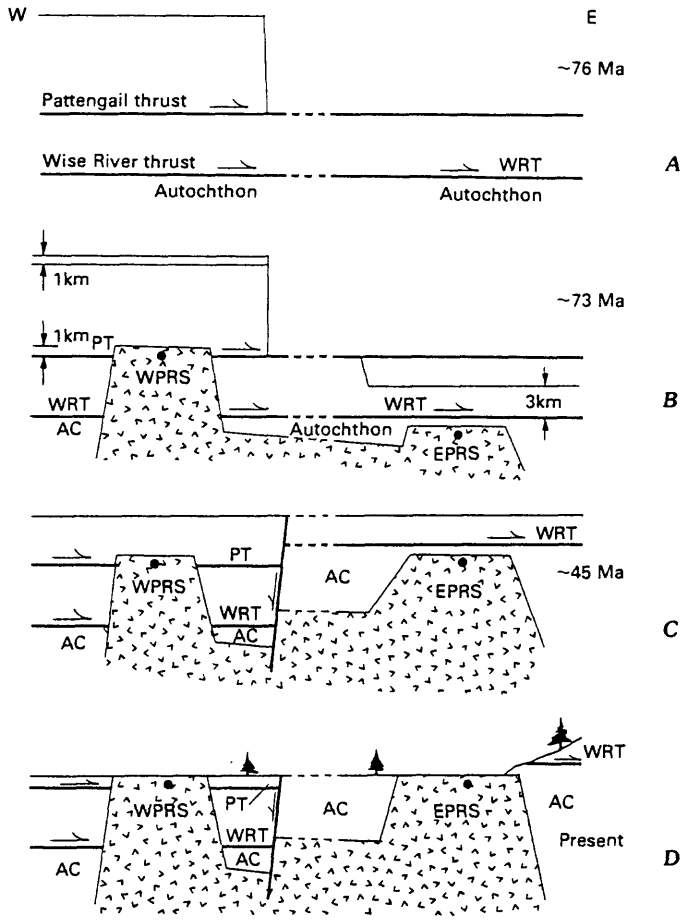

Figure 2. Schematic representation of the sequence of thrusting, erosion, igneous intrusion, and high-angle faulting in the Pioneer Mountains. (A), arrival of the thrust sheets. (B), emplacement of the plutons; their tops are arbitrarily set at the present level of erosion. (C), displacement on the Fourth of July fault system downdropping the west Pioneer block. (D), erosion to the present time. EPRS and WPRS are the two reference sites. Dotted lines schematically connect the panels for the west and east Pioneers. Long dashed lines on (B) are the original surfaces of the thrust sheets, and the distance between a given dashed line and the next lower solid line defines the amount of crust removed by erosion up to the specified time. The upper thrust plate rests on the Pattengail thrust (PT); the lower thrust plate rests on the Wise River thrust (WRT; Zen, 1988b), which rests on the autochthon (AC).

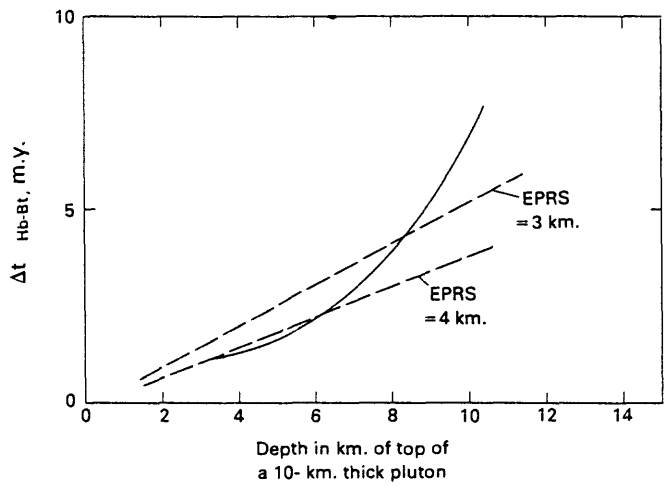

Figure 3. Nominal cooling history of a pluton given by the difference between the argon spectrum ages of hornblende and biotite ($\hat{}t_{hb-bt}$), as a function of depth of intrusion. Distance from sample location (WPRS) to the margin of the pluton, assumed to be the roof, is 0.5 km. Solid curve, calculated from conduction model of heat flow. Dashed curves, linear cooling model used by Snee (1982).

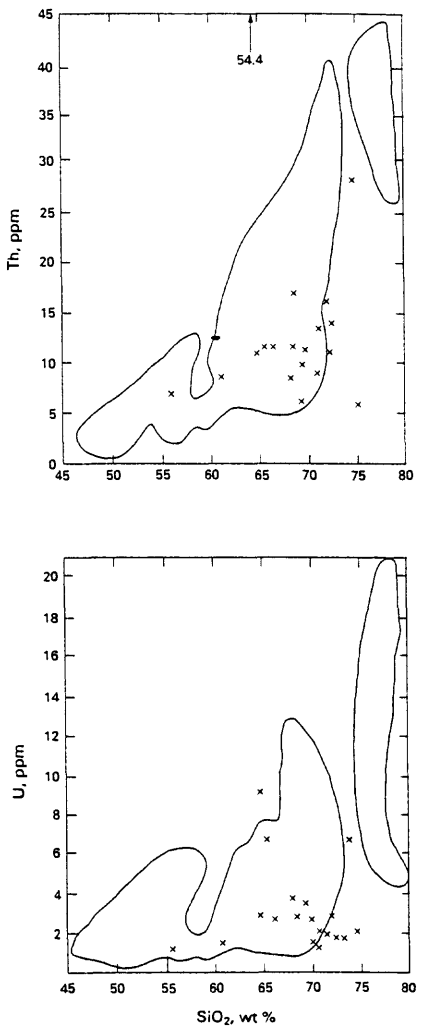

Figure 4. SiO_2 versus thorium and uranium contents of the Pioneer batholith rocks, and comparison with the Boulder batholith rocks shown generalized as a distribution field (Tilling and Gottfried, 1969).

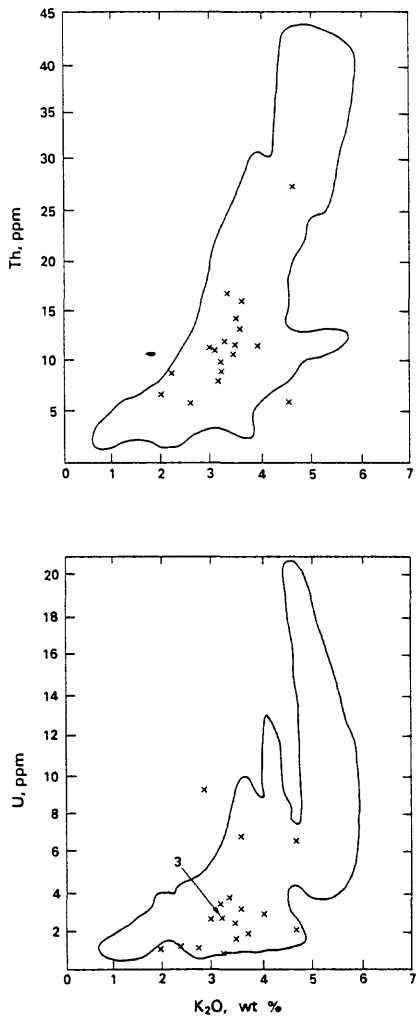

Figure 5. Thorium and uranium contents versus K_2O content of Pioneer batholith, and comparison with the Boulder batholith rocks shown generalized as a distribution field (Tilling and Gottfried, 1969). The number "3" refers to triplication of data points.

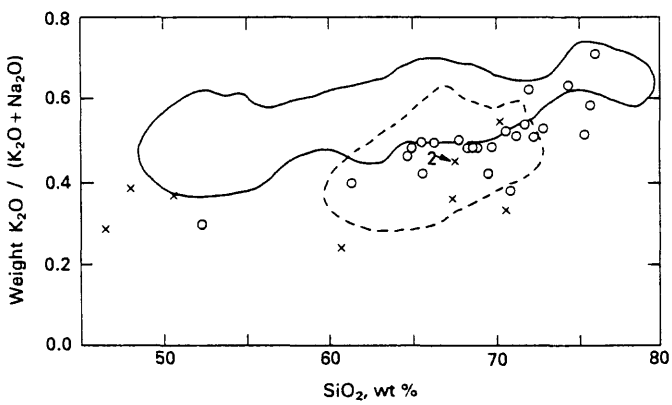

Figure 6. Weight percent SiO_2 versus $K_2O/(K_2O+Na_2O)$ plot of Pioneer batholith rocks (circles) and of the Proterozoic gneiss-and-amphibolite unit (Xga, crosses), compared to the Main Series (solid line) and the Sodic Series (dashed line) of the Boulder batholith (Tilling, 1973). The number "2" refers to duplication of data points.

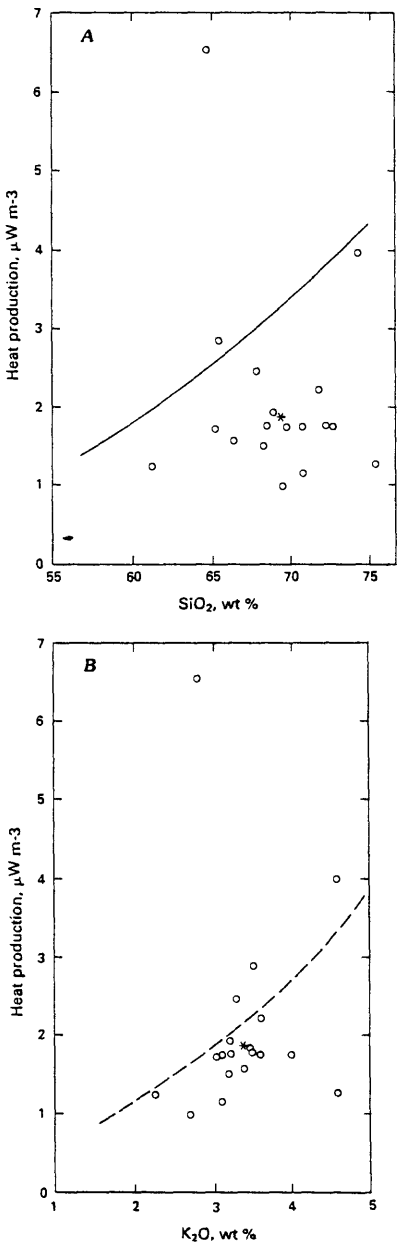

Figure 7. (A) SiO_2 and (B) K_2O contents versus heat productivity. Comparison of Pioneer batholith rocks with those of the Boulder batholith, shown as the trend line given by Tilling and others (1970). Average values for the Pioneer batholith rocks (n=17) excluding one anomalous value are given by stars.

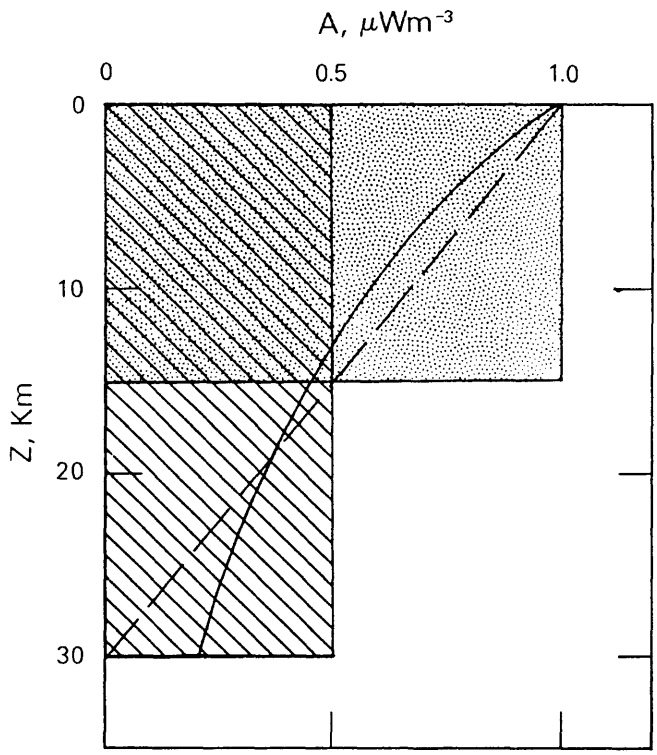

Figure 8. Four possible distributions of heat productivity, A, in the crust. (A), A=1 uW.m^{-3}, confined to the upper 15 km only, A=0 below that depth. (B), A=0.5 uW.m^{-3}, distributed throughout the 30 km of crust, so that the integrated value of A for the entire crust remains the same. (C), A=1 uW.m^{-3} at Z=0, decreasing linearly to A=0 at Z=30, so that the integrated value of A for the entire crust remains the same. (D), $A=A_o e^{-Z/D}$; where A_o=1 uW.m^{-3} and D=18.825, so that the integrated value of A for the entire crust remains the same.

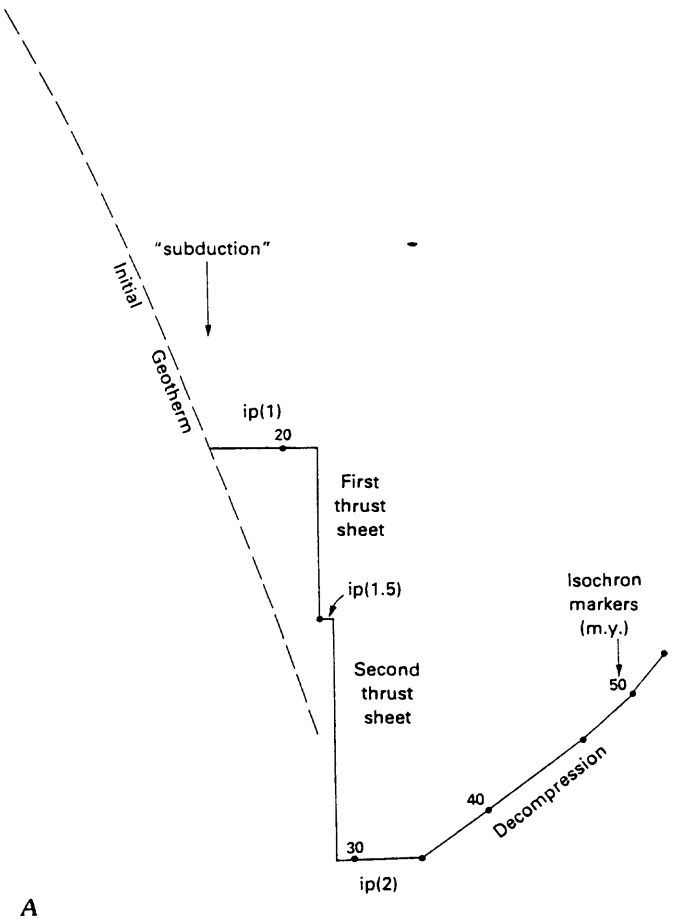

Figure 9 (A). Key relating tectonic events and incubation periods to changes in the curves for temperature evolution at chosen depths. See text for discussion; see Table 3 for model parameters.

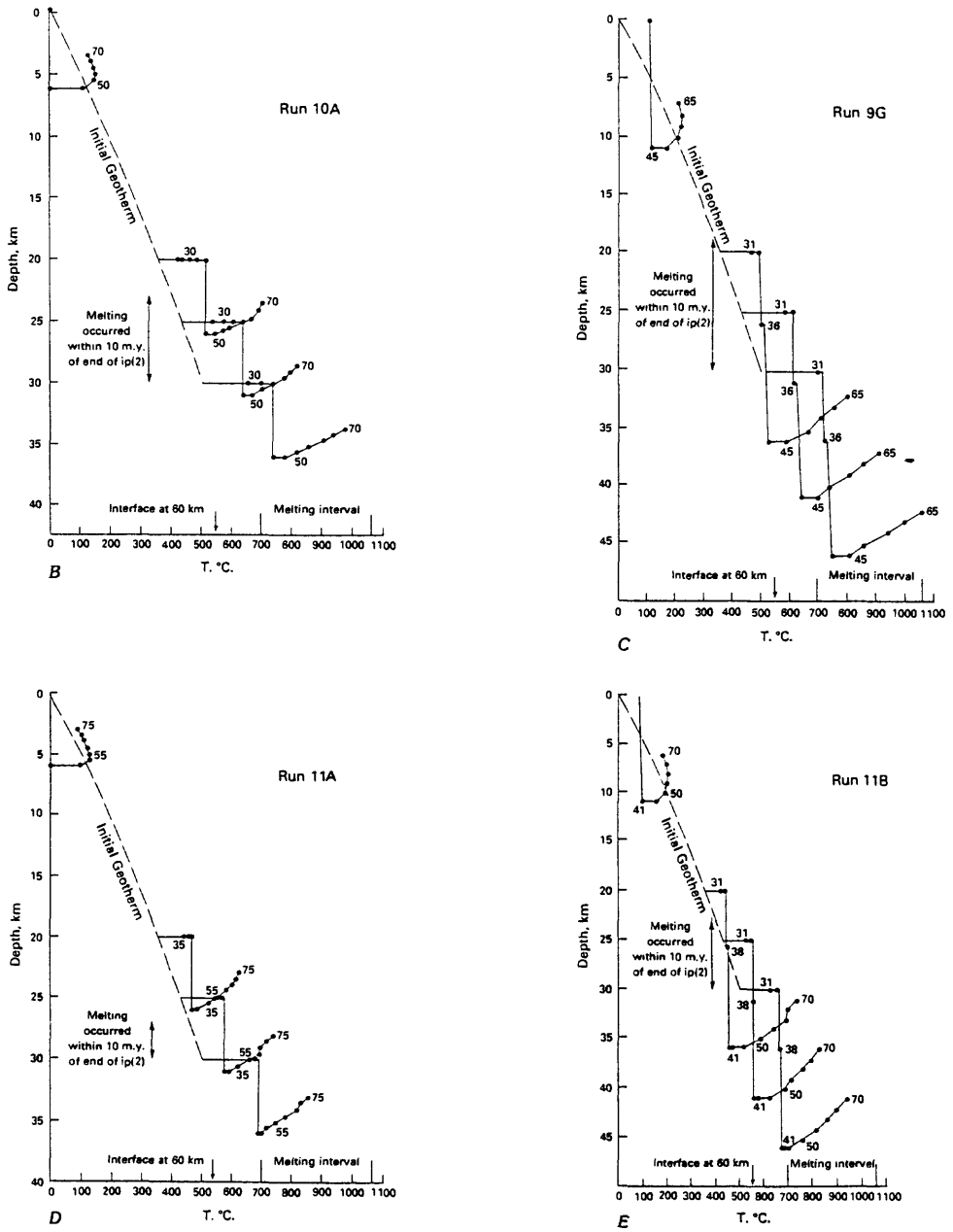

Figure 9 (B) through (E). Temperature evolution at chosen depths for four selected runs. (B), Run 10A. (C), Run 9G. (D), Run 11A. (E), Run 11B.

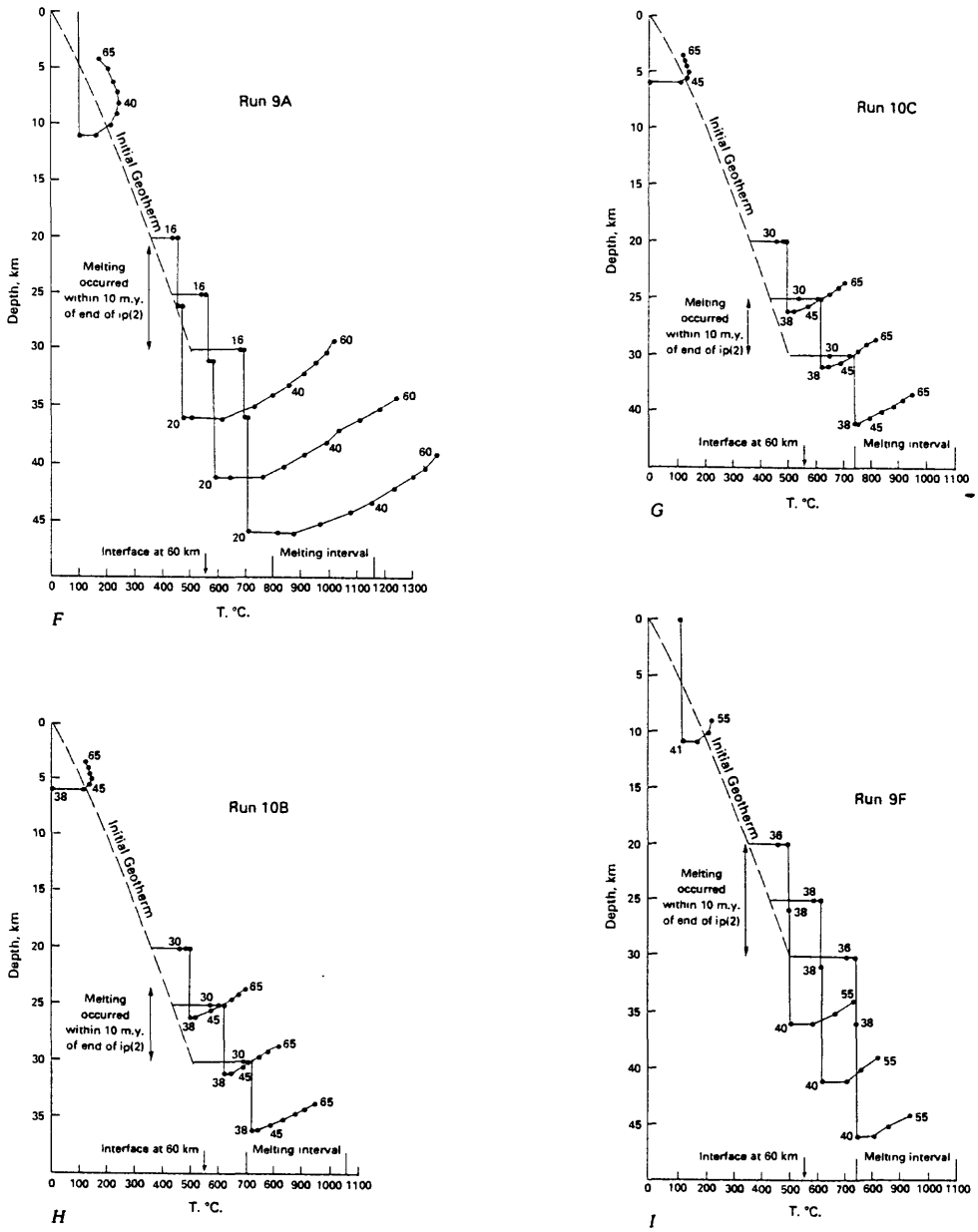

Figure 9 (F) through (I). Temperature evolution at chosen depths for four selected runs. (F), Run 9A. (G), Run 10C. (H), Run 10B. (I), Run 9F.